Factors controlling porosity in Upper Carboniferous–Lower Permian carbonate strata of the Barents Sea

S. N. Ehrenberg

ABSTRACT

A 300-m (1000-ft)-thick succession of shallow- and warm-water carbonates has been studied in well cores from the southernmost Barents Sea, offshore north Norway. These upper Paleozoic strata contain numerous zones of moderate to high porosity, including a wide range of depositional facies, despite moderately high burial temperatures and the absence of petroleum charge. Most porosity appears to be either primary or created during early (eogenetic) diagenesis. Negative correlation between porosity and both bulk-rock alumina content and stylolite frequency reflects the influence of phyllosilicate minerals in localizing stylolitic dissolution. This provides part of the explanation for the overall correlation between porosity and the platform's stratigraphic evolution. The early stage of mixed siliciclastic-carbonate deposition has low porosity because of extensive chemical compaction in aluminous beds. The following siliciclastic-poor stage shows upward-increasing porosity associated with aggradation of muddy buildups and wackestones, followed by the progradation of a more proximal facies belt of thinly bedded dolomitic mudstones. Maximum porosity development occurs in the overlying, little-dolomitized grain-shoal facies belt, which shows upward decrease in porosity because of a transgressive trend that developed progressively lower energy depositional conditions, favoring the occurrence of stylolite-prone shaly laminations. A general porosity-favorable factor is the presence of a stratified column of high-salinity brine, enforcing a closed diagenetic system during burial. Limestones and dolostones comprising this platform have very different proportions of low and high porosity values. Limestones have positively skewed frequency distribution (many samples <5% porosity), whereas dolostones have higher average porosity with symmetric distribution (few samples <5% porosity). The low limestone porosities result from cementation by coarse calcite-spar in grain-dominated samples and matrix compaction and cementation

Manuscript received December 4, 2003; provisional acceptance May 6, 2004; revised manuscript received June 21, 2004; final acceptance July 19, 2004.

AUTHOR

S. N. Ehrenberg ~ *Statoil, N-4035 Stavanger, Norway; sne@statoil.com*

Steve received a Ph.D. from the University of California at Los Angeles in 1978. He works on sandstone and carbonate petrology, sedimentology, and stratigraphy.

ACKNOWLEDGEMENTS

My coauthors on previous Finnmark Platform papers, Tore Svånå, Erik Broe Nielsen, Lars Stemmerik, Neil Pickard, Norman Oxtoby, Inger Nilsson, and Vladimir Davydov, are acknowledged for their contributions to establishing the basis for this study. An unpublished 1992 study for Conoco by Ray Mitchell provided the first descriptions of the 7128/6-1 cores and has been a valuable reference. Erling Siring wrote the computer programs used to produce the running averages in Figure 9 and the variograms in Figure 16. Norman H. Oxtoby (Department of Geology, Royal Holloway, University of London) performed the fluid-inclusion measurements depicted in Figure 8. The manuscript has benefited from reviews by Jim Jennings, Jesper K. Nielsen, Neil A. H. Pickard, Gretchen M. Gillis, Ronald A. Nelson, and F. Jerry Lucia.

in muddy facies, features that are less common in dolostones possibly because of lesser propensity for stylolite development and the resistance of early-dolomitized matrix to compaction.

INTRODUCTION

This study examines the causes of porosity variation in a succession of shallow- and warm-water carbonates of late Moscovian to early Sakmarian age (equivalent to Desmoinesian–Wolfcampian in North American nomenclature; Figures 1–5). An important feature of these strata is the occurrence of potentially economic thicknesses of strata with moderate to high porosity. Based on routine core analyses of 1-in. (2.5-cm) horizontal plugs spaced three per 1 m (3.3 ft), 25% of the cored 297 m (974 ft) of this section in well 7128/6-1 (drilled by Conoco) has porosity greater than 15%, with the average porosity of these higher porosity plugs being 20% (maximum 34%). Comparison with the porosity-depth trend in shallow-water carbonates of south Florida (Figure 6) indicates that these porosities are relatively high for their depth and temperature history. As in most of the south Florida section, the Finnmark Platform pore spaces contain no petroleum, and the rarity of fluorescent (petroleum-filled) fluid inclusions (Ehrenberg et al., 2002) suggests that this has been the case throughout geological time. Therefore, inhibition of cementation by petroleum is ruled out as an explanation for high porosity, and other relationships can be considered.

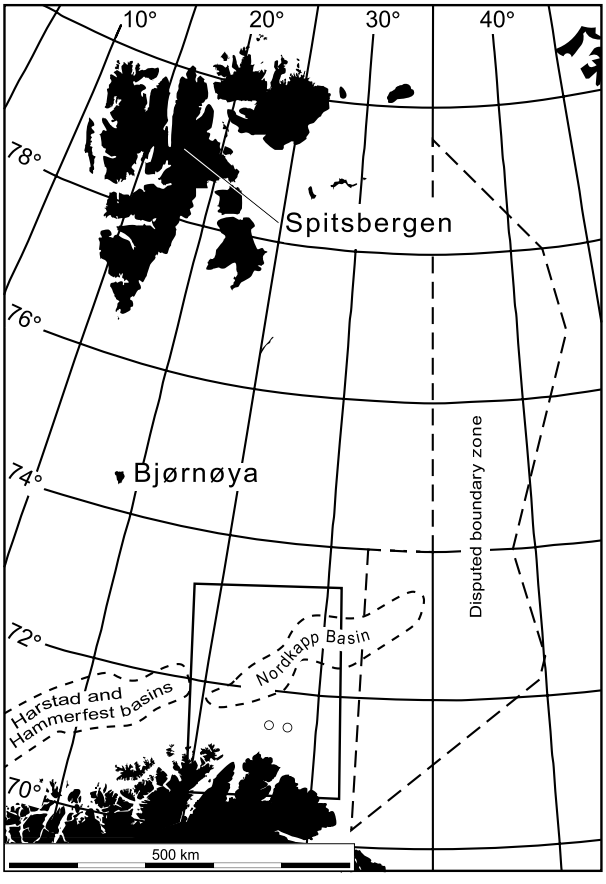

Figure 1. Barents Sea map, with location of the detailed map of Figure 2. Circles show locations of the two wells studied. The Svalbard Archipelago includes the islands shown north of 74° latitude and west of 35° longitude. Modified from Ehrenberg et al. (2002) with permission from the Society for Sedimentary Geology.

Modeling and prediction of carbonate diagenesis and reservoir quality remains a field where quantitative calibration of basic processes and even ranking of their relative importance are incipient and uncertain, despite a plethora of general models and case histories (Tucker and Wright, 1990; Budd et al., 1995; Montañez et al., 1997; Moore, 2001). The present study is relevant to petroleum exploration and production because quantitative relationships observed between factors controlling porosity of Finnmark Platform carbonates may have broad applicability to understanding porosity distributions of carbonates in general. Furthermore, the upper Paleozoic carbonates of the Barents Sea constitute an important potential frontier petroleum province (Doré, 1995), and the cored intervals in well 7128/6-1 are regarded as the type section for much of these strata throughout the Norwegian sector (Larssen et al., 2002). Depositionally similar and roughly age-equivalent carbonates also form major petroleum reservoirs in the Timan-Pechora province of northern Russia, some 1200 km (750 mi) to the east (Martirosyan et al., 1998). Insofar as the 7128/6-1 cores are indeed representative of this important prospective reservoir interval, the results from the present study are likely to have broad relevance throughout this arctic region.

The results presented are based on a series of thin sections and bulk chemical, stable isotope, and x-ray diffraction analyses at a constant, approximate 1-m (3.3-ft) sampling interval, each sample coinciding with horizontal plug measurements of porosity, permeability, and grain density. Previous papers have described the stratigraphy, diagenesis, and inorganic geochemistry of these strata (Bugge et al., 1995; Ehrenberg et al., 1998a; b; 2000; 2001; 2002; Ehrenberg and Svånå, 2001). Porosity in the following text refers to total percent porosity measured by helium porosimetry, and

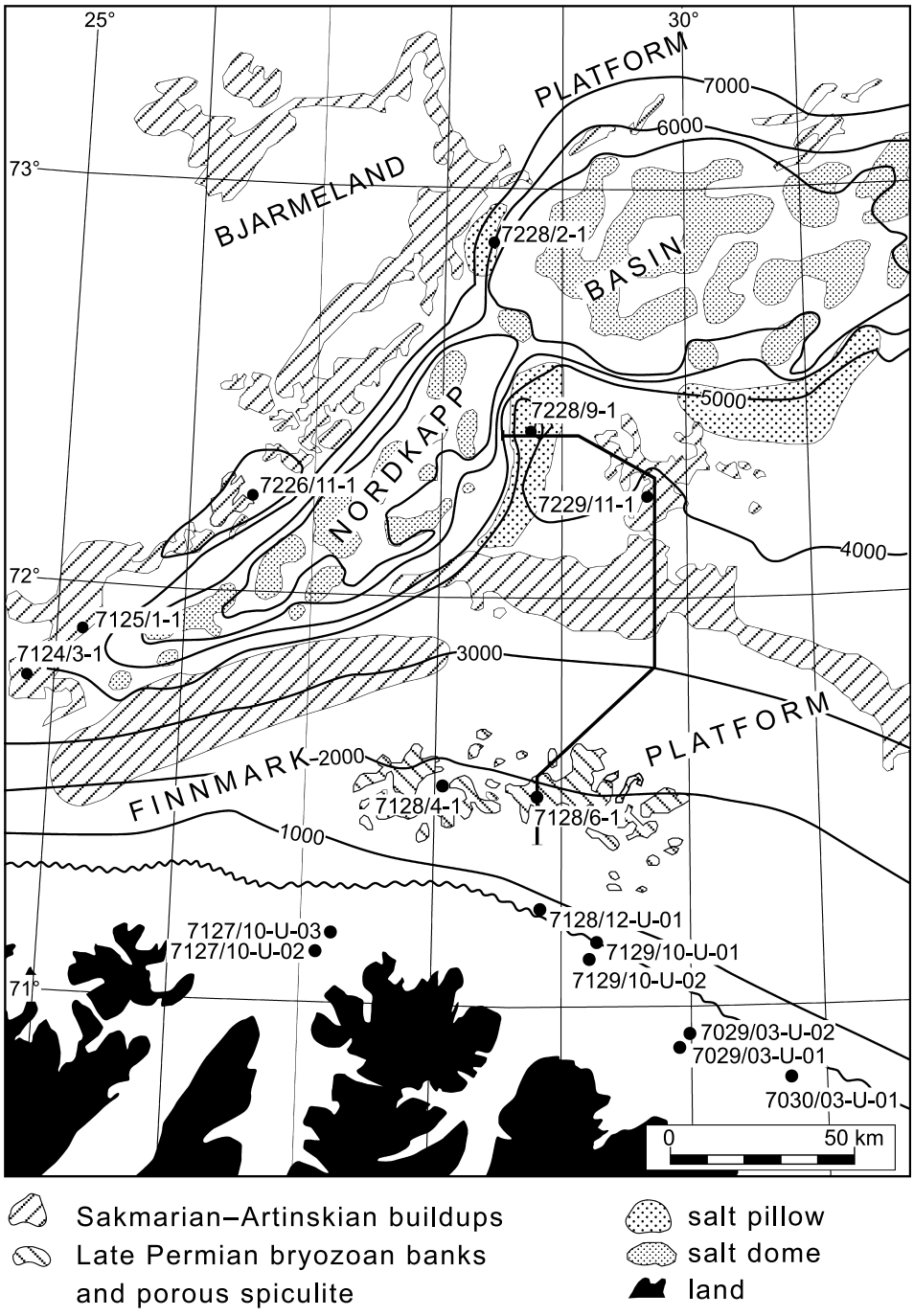

Figure 2. Map of Finnmark Platform and surroundings, showing well locations, 1000-m (3280-ft) depth contours on top Permian surface, and location of cross section in Figure 3 (line northward through well 7128/6-1). Points south of 71° 15′ latitude are locations of shallow stratigraphic test cores. Wiggly line represents southward erosional termination of carbonate strata. Modified from Ehrenberg et al. (1998a) with permission from the Geological Society of Norway.

permeability refers to Klinkenberg-corrected gas permeability, both from horizontal 1-in. (2.5-cm) plugs. Permeability-porosity relationships are not the focus of this paper but have been discussed briefly in Ehrenberg et al. (1998b).

Throughout this paper, the pedantic distinction between European and North American timescale nomenclature is observed by giving European system and stage names first followed by North America equivalents in parentheses.

GEOLOGIC SETTING

In Late Carboniferous to Permian time, the Barents Sea was part of a vast province of carbonate-dominated deposition that extended from the Canadian arctic to northern Russia (across the northern margin of Pangea) and thence southward to the Caspian Sea (Stemmerik, 2000; Ford and Golonka, 2003). The segment of this province bordering the coast of northern Norway is the Finnmark carbonate platform (Figures 1–3). This

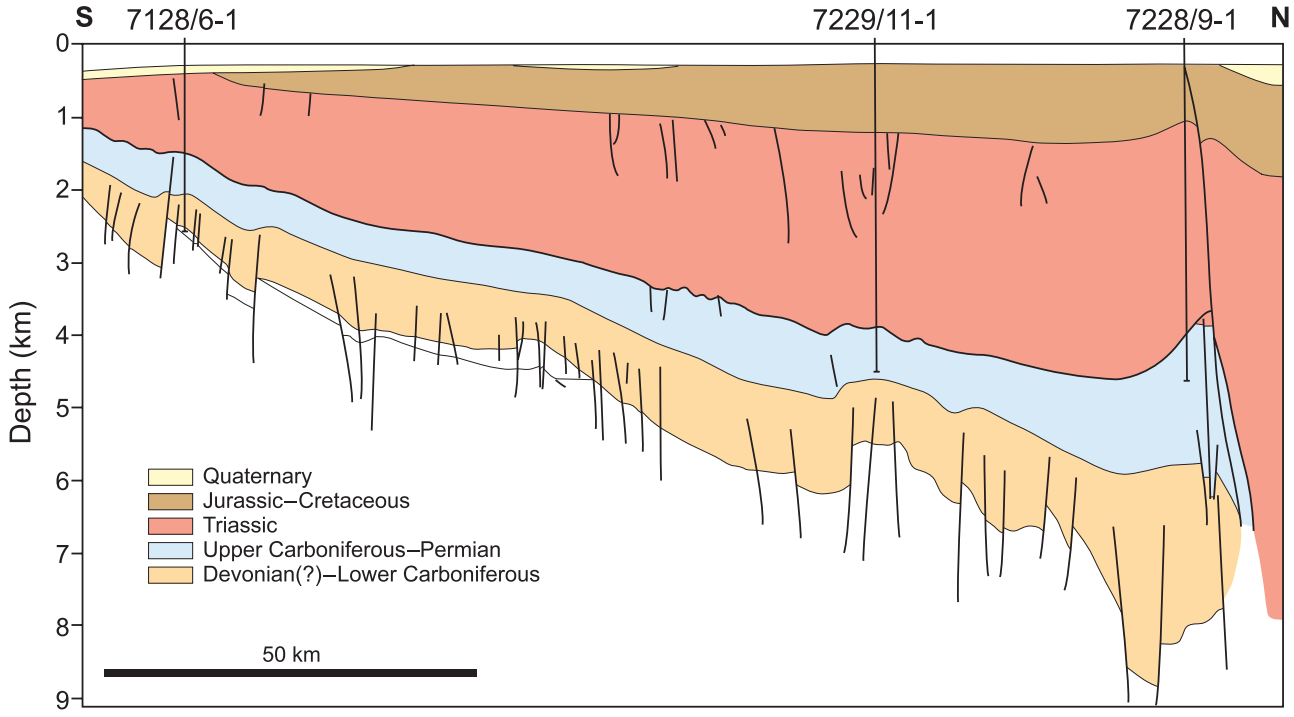

Figure 3. Geologic cross section based on seismic lines from inner Finnmark Platform to Nordkapp Basin. Line of section is shown in Figure 2.

segment is bounded to the south by erosional subcrop onto the Fennoscandian craton and to the north by the downfaulted Nordkapp Basin, where the platform carbonates pass laterally into evaporites and deep-water facies.

Three main tectonic episodes have affected this area (Nyland et al., 1992; Nilsen et al., 1993):

1. The major structural elements of tilted fault blocks and half grabens formed during Early Carboniferous (Mississippian) extension. The postrift, Upper Carboniferous (Pennsylvanian)–Permian carbonate-platform succession rests relatively undisturbed over the faulted Visean–Bashkirian (Meramecian–Morrowan) siliciclastics.
2. Early Cretaceous reactivation exaggerated preexisting structures, such that Early Carboniferous grabens were again the sites of greatest subsidence.
3. Early Tertiary uplift and erosion enhanced the already pronounced northward tilting.

Today, the upper Paleozoic strata form a monocline that dips approximately 2° northward at top Permian level as a result of both northward thickening of individual units and increasing uplift toward the mainland.

In the area of the exploration wells studied, roughly 0.8–1.5 km (0.5–0.9 mi) of Mesozoic strata eroded during the early Tertiary uplift. Basin modeling results indicate that maximum burial temperatures in the subject strata were in the range of roughly 90–100°C throughout much of Tertiary time (K. Lindbo, 2002, personal communication), consistent with the trend of vitrinite reflectance with depth, which has values of 0.6–0.7 R_o in the Upper Carboniferous–Lower Permian carbonate interval (Ehrenberg et al., 1998b). Present temperatures are estimated to be 60–75°C, and fluid pressures are only slightly above hydrostatic.

STRATIGRAPHY

The stratigraphy is divisible into the main units shown in Figure 3. These rest upon a basement that consists of low-grade metasediments of possibly Devonian to upper Precambrian age in the area of the wells studied. The oldest known strata there are Visean–Bashkirian (Meramecian–Morrowan) nonmarine to marine siliciclastics (339 m [1112 ft] thick in well 7128/6-1, but thicker in adjacent half grabens). These were deposited both before and during the Early Carboniferous (Mississippian) extensional tectonic episode noted above.

Following rifting, the Upper Carboniferous (Pennsylvanian) to Upper Permian Finnmark carbonate platform was deposited (527 m [1729 ft] thick in well 7128/6-1, but thickening northward to 1300 m [4265 ft] near the Nordkapp Basin; Figure 2). The top Permian surface is sharply overlain by Mesozoic deep-marine siliciclastics (eroded to 1135-m [3724-ft] thickness in well 7128/6-1, but thickening to 4 km [2.5 mi] northward of the Pliocene–Pleistocene unconformity). Finally, a thin veneer of Quaternary glacial debris (129 m [423 ft] in 7128/6-1) covers the lower Tertiary unconformity over much of the southern Barents Sea.

Within the Finnmark carbonate platform, four distinct stages of depositional evolution are recognized (Ehrenberg et al., 1998a):

1. Upper Carboniferous (Pennsylvanian) mixed siliciclastic-carbonate deposits, reflecting waning tectonic activity and decreasing topographic relief; siliciclastic input to this lower part of the platform succession is reflected in the high gamma-ray activity and bulk-rock alumina content corresponding to lithostratigraphic units L-1 to L-3 (2150–2020 m in well 7128/6-1; Figure 4)
2. dominantly Lower Permian cyclic warm-water carbonates containing frequent algal buildups and abundant dolomite and anhydrite (2020–1836 m in well 7128/6-1; Figure 4)
3. upper Sakmarian to Kungurian (uppermost Wolfcampian–middle Leonardian) cool-water carbonates, including bryozoan-echinoderm grainstones to wackestones in the inner to middle platform (unit L-8 in well 7128/6-1) and major bryozoan mud mounds in deeper water, near the Nordkapp Basin (Figure 2)
4. Kungurian (middle Leonardian)–Upper Permian cold-water spiculite, carbonate, and siliciclastic deposits (Ehrenberg et al., 2001), abruptly terminated by massive siliciclastic influx in the earliest Triassic

As discussed by Beauchamp and Desrochers (1997) for broadly equivalent strata of arctic Canada, the stepwise replacement of warm-water biota by progressively cooler water biota from stages 2 to 4 records climatic cooling along the northern margin of Pangea, partly in response to increasing paleolatitude (from around 18°N in the Late Carboniferous to 38°N at the end of the Permian; Steel and Worsley, 1984) but probably also reflecting changes in oceanic circulation patterns. Attending cooling, water depths increased over large parts of these platforms. Thus, the Finnmark carbonate platform shows an evolutionary trend from warm-water, photozoan (James, 1997) depositional conditions in the Late Carboniferous to early Sakmarian to cool-water heterozoan conditions in the late Sakmarian to Late Permian.

PREVIOUS WORK

By far, the most complete and extensively sampled stratigraphic section of upper Paleozoic carbonates in the entire Barents Sea region is represented by the cores from well 7128/6-1 (440 m of the 527-m Upper Carboniferous to Upper Permian succession). The comprehensive coring program in this 1991 well was mandated by the Norwegian Petroleum Directorate to provide an upper Paleozoic reference section supplementing a much thinner stratigraphic section previously assembled from several shallow drill holes (Figure 2) near the erosional termination of the carbonate platform against the Norwegian mainland (Bugge et al., 1995; Ehrenberg et al., 2000). Another 51 m (167 ft) of core from a critical portion of the section was recovered in well 7128/4-1, drilled in 1994 (by Statoil) some 26 km (16 mi) due west of well 7128/6-1 (Figure 4). Stratigraphically equivalent carbonates have also been cored elsewhere in the Norwegian part of the Barents Sea, notably in wells 7120/2-1 and 7226/11-1 (Lønøy, 1988; Cecchi, 1993; Cecchi et al., 1995), and are exposed on the Svalbard archipelago, where they have long been used in oil-industry training exercises as outcrop analogs for the Barents Sea subsurface (Figure 5).

Ehrenberg et al. (1998a, b) divided the carbonate-platform succession of well 7128/6-1 into nine lithostratigraphic units, designated L-1 to L-9 (Figure 4). A hierarchy of depositional sequences was recognized based on patterns of variation in facies and cycle thickness. The two largest scale sequences span late Moscovian (Desmoinesian) to Late Permian time and are thus ''supersequences'' of ''second-order'' magnitude, according to the terminology of Fitchen (1997). Each of these intervals comprises three to four third-order sequences, designated S-1 to S-7 (Figure 4). Analysis of fusulinid biostratigraphic data by the method of graphic correlation indicates that sequences S-2 to S-5 have individual durations of 7–9 m.y. (V. Davydov, 2001, personal communication).

The subject of the present paper is the lower, photozoan part of the Finnmark Platform succession,

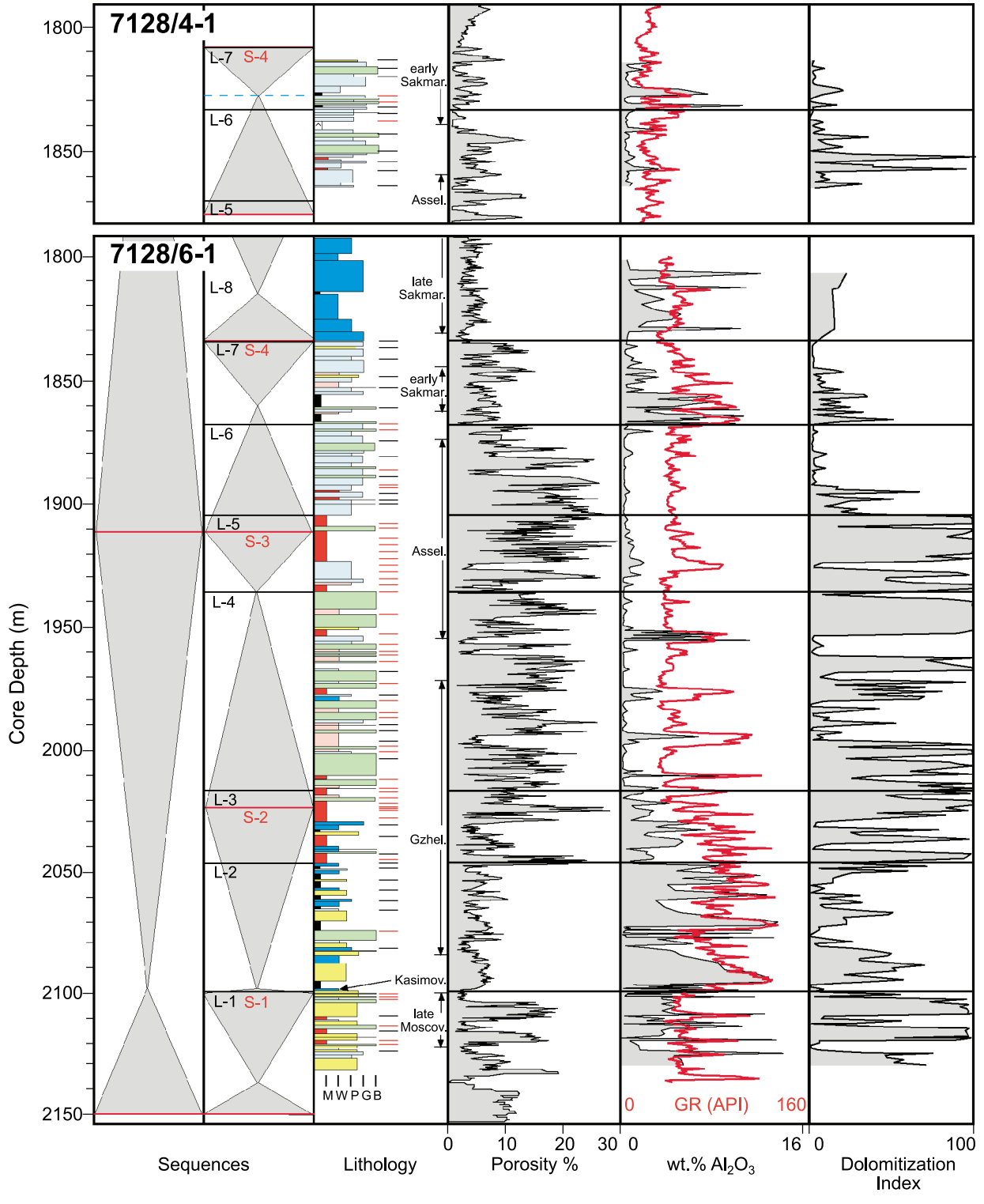
7128/4-1
7128/6-1
Core Depth (m)
1800
1850
1900
1950
2000
2050
2100
2150
L-7 S-4
L-6
L-5
L-8
S-3
L-4
L-3
S-2
L-2
L-1 S-1
early Sakmar.
Assel.
late Sakmar.
Gzhel.
Kasimov.
late Moscov.
M W P G B
0 GR (API) 160
0 10 20 30
0 16
0 100
Sequences
Lithology
Porosity %
wt.% Al2O3
Dolomitization Index
Lithology:
bryozoan grain/ packstone and wackestone
foraminifera grainstone and packstone
dolomitic mudstone
fusulinid wackestone
buildup
shale and marl
siltstone and sandstone
L-5
lithostratigraphic unit boundary
S-4
sequence boundary
cycle top
exposure surface

including lithostratigraphic units L-1 to L-7, which comprise sequences S-1 to S-4 (Figure 4). These sequences, in turn, consist of numerous smaller scale cycles, some of which themselves contain yet smaller cycles. Consistent with the model of Schlager (2004), cycle tops are defined by possible exposure surfaces, flooding surfaces, or commonly both (Figure 4), and the time intervals represented by individual cycles are likely to vary across a wide spectrum of magnitudes. This interval corresponds to the Gipsdalen Group in the new stratigraphic nomenclature of the Barents Sea subsurface (Larssen et al., 2002), including the Falk Formation (units L-1 and L-2) and the Ørn Formation (units L-3 to L-7). These strata contain numerous high-porosity zones in wells 7128/4-1 and 7128/6-1 and are regarded as highly prospective for reservoir quality throughout the Barents Sea province (Stemmerik et al., 1999).

Except for local occurrences of porous spiculitic chert at the very top of the succession, the upper, heterozoan part of the succession has low porosity because of a combination of shaly composition and extensive burial cementation. This interval includes unit L-8 (Isbjørn Formation; upper Sakmarian–Artinskian) and unit L-9 (Røye Formation; Kungurian–Upper Permian). The diagenesis of these strata is treated elsewhere (Ehrenberg et al., 1998b, 2001).

Arid climatic conditions during deposition of the Gipsdalen Group are indicated by the common presence of calcium sulfate and early, evaporite-related dolomite, restricted biotic assemblages suggestive of hypersaline conditions, lack of pronounced soil horizons, and apparent absence of negative carbon isotope excursions associated with inferred exposure surfaces at cycle tops (Stemmerik and Larssen, 1993; Stemmerik et al., 1999; Ehrenberg et al., 2002). In the area of the wells studied, the Gipsdalen Group represents an inner to middle platform setting. Possible low-relief platform margins may be located further northward, but are poorly defined and difficult to correlate on seismic lines. The Gipsdalen Group is thus regarded as comprising a ramp-type platform in this area, such that diagenesis may best be compared with the arid ramp models of Moore (2001).

Twelve broad facies categories were defined by Ehrenberg et al. (1998a) comprising the Upper Carboniferous–Permian strata of wells 7128/4-1 and 7128/6-1, ten of which are represented in the present study (Table 1). Based on the sampling strategy of fixed 1-m (3.3-ft) spacing used in this study and the nearly complete core coverage of the interval of interest, proportions of samples should be statistically representative of the relative proportions of the facies present in the stratigraphic section and the pore types present in each facies (Table 1). The facies relationships and depositional model for these Finnmark Platform cores are similar to those described in the more detailed scheme of Morin et al. (1994) for Lower Permian strata of arctic Canada. Figure 4 summarizes the distribution of these facies in the cored intervals. Photomicrographs of porosity and cement types in four samples representative of porosity-prone facies are shown in Figure 7.

PARAGENESIS AND PORE TYPES

Calcite cements throughout the Gipsdalen Group of the exploration wells consist mainly of an early generation of fine spar (<0.1 mm; <0.004 in.) and a later generation of coarse-blocky spar (0.1–1 mm; 0.004–0.04 in.). The fine spar lines bioclasts and bioclast molds and is interpreted as a near-surface (eogenetic; Choquette and Pray, 1970) cement; it is overgrown by the coarse spar, which is interpreted as a burial (mesogenetic) cement (Ehrenberg et al., 2002). Coarse spar in or near clay-rich beds tends to have crystal zones with more Fe-rich compositions than cements more distant from shaly beds.

Dolomite in the studied interval is broadly categorized as fine dolomite (<0.1 mm), coarse dolomite (0.1–1 mm), and saddle dolomite (0.1–2 mm). Fine dolomite includes both xenotopic-cloudy matrix-replacive dolomite and euhedral-limpid cement crystals. In extensively dolomitized mudstones and wackestones, these two end-member varieties of fine dolomite commonly occur intimately associated in volumes originally occupied by carbonate mud. In little-dolomitized packstones, grainstones, and sandstones, fine dolomite

Figure 4. Sequence-stratigraphic interpretation, core description, and profiles of porosity, bulk-rock alumina content, gamma-ray activity, and dolomitization index (DI = 100 × dolomite/total carbonate), in cored intervals of the Gipsdalen Group of wells 7128/4-1 and 7128/6-1. Age constraints from fusulinid dating (Ehrenberg et al., 2000) are shown as arrow brackets. Porosity profile shows plug measurements in cored intervals and wire-line–log porosity outside of core coverage. Modified from Ehrenberg et al. (2002) with permission from the Society for Sedimentary Geology.

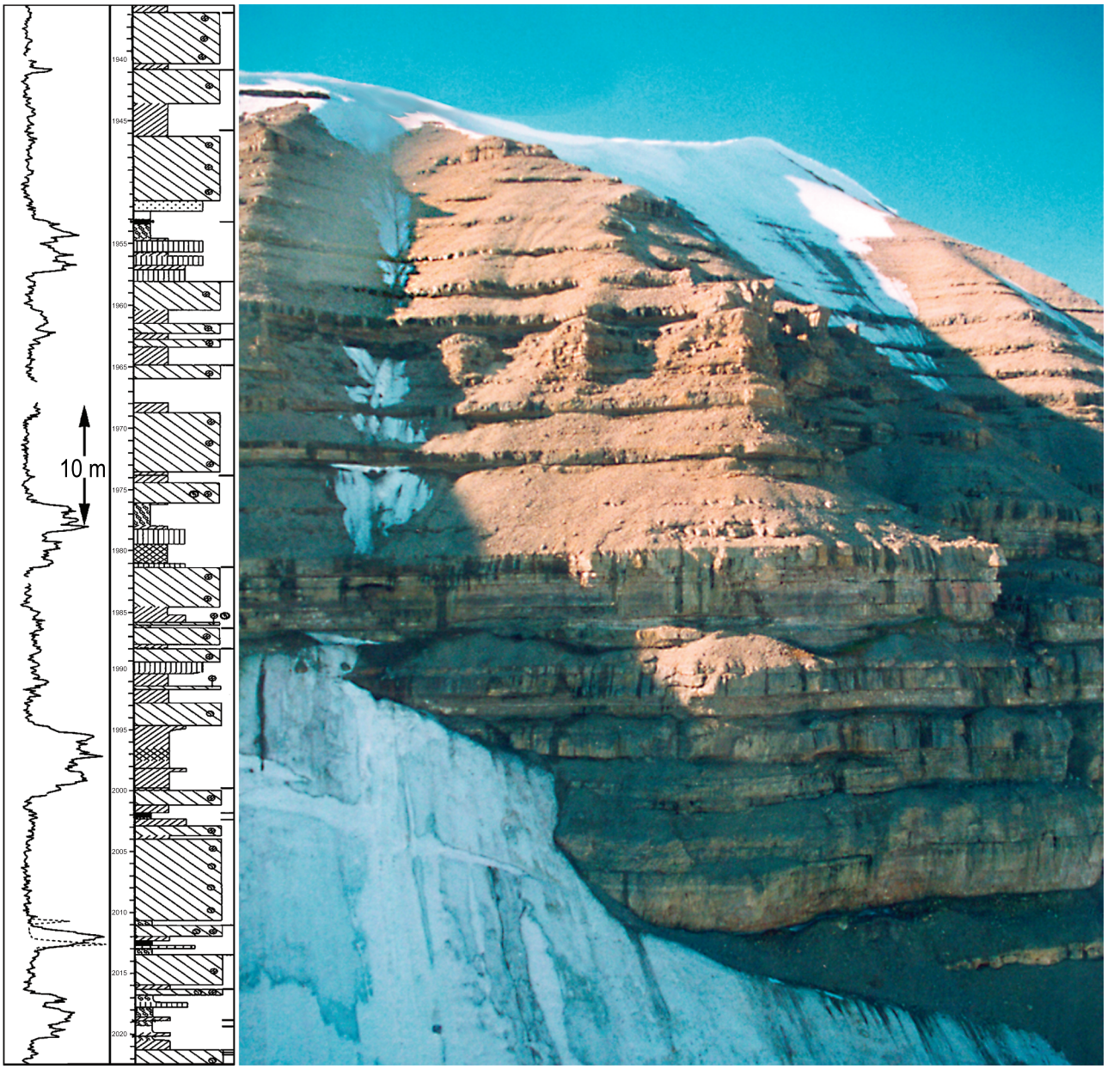

Figure 5. Comparison between gamma-ray log (left track; 0–150° API) and core description through unit L-4 of well 7128/6-1 (Ehrenberg et al., 1998a, with permission from the Geological Society of Norway) and a photograph of stacked wackestone and buildup cycles of similar age exposed on Spitsbergen. Meter and decimeter heterogeneity of these strata reflects varying hierarchic scales of depositional cyclicity.

is localized in intergranular areas of former carbonate mud.

Coarse dolomite is commonly a major constituent of extensively dolomitized buildup and grain-dominated lithologies but is minor to absent elsewhere. Coarse dolomite consists of clear euhedral rhombs that fill pore spaces and also replace matrix and bioclasts. Cathodoluminescence petrography reveals that coarse dolomite crystals commonly formed as overgrowths on more strongly luminescent fine dolomite rhombs and are concentrically zoned. Saddle dolomite is common in limestone beds of units L-1 and L-2 but is absent to minor in overlying units. Saddle dolomite is associated with coarse anhydrite cement, and both phases commonly truncate crystal zoning in coarse calcite spar.

Homogenization temperatures of primary, two-phase aqueous fluid inclusions range from 52 to 117°C in coarse-blocky and syntaxial calcite cements and

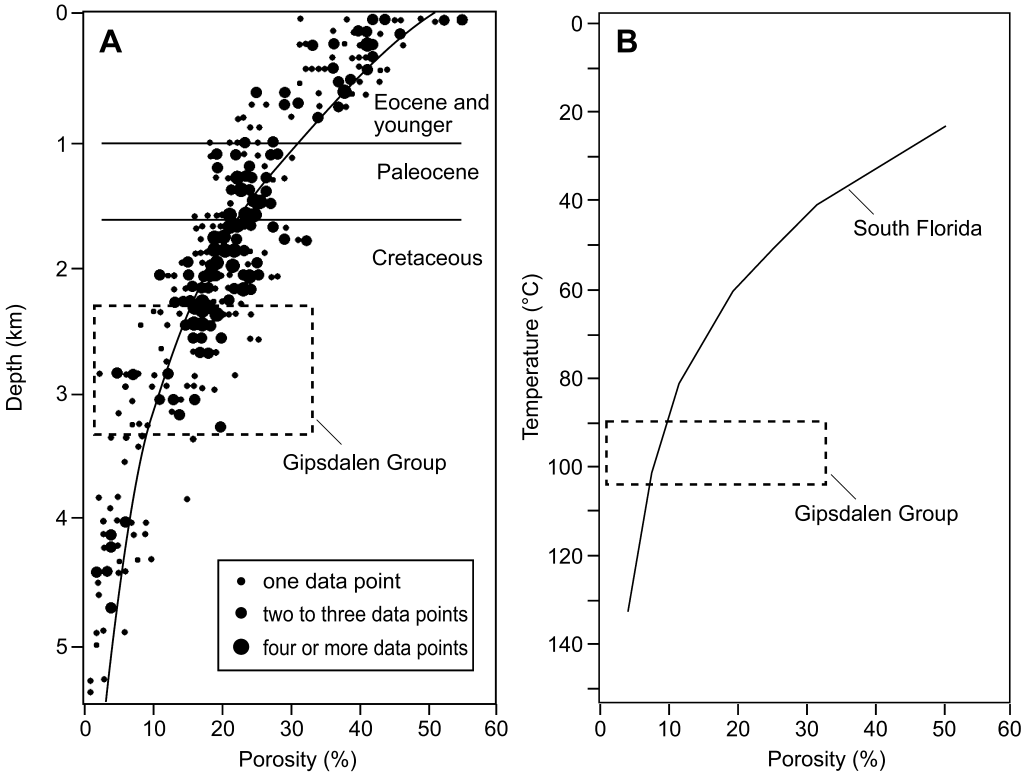

Figure 6. Comparison of porosity range, maximum burial depth, and maximum temperature range in Finnmark Platform cores (Gipsdalen Group) with south Florida limestone data of Schmoker and Halley (1982). (A) Porosity-depth trend; (B) porosity-temperature trend, based on geothermal gradient of 18°C/km. For its burial and thermal history, much of the Finnmark Platform section has anomalously high porosity compared with the south Florida strata.

81–117°C in coarse and saddle dolomite cements, consistent with continuous cement growth over a wide temperature span (Ehrenberg et al., 2002). The freezing temperatures of these fluid inclusions further indicate that original pore waters were replaced by high-salinity brine (mostly 15–20 wt.% NaCl equivalent; four to six times seawater salinity) before burial cementation began. These data define part of a larger scale trend of increasing salinity with depth through the entire upper Paleozoic section (Figure 8).

Relative proportions of different pore types vary widely between different facies and also between the individual plugs comprising each facies category. Pore-type proportions, as qualitatively estimated from thin sections, are listed in Table 1 for samples with porosity greater than 10%. Essentially, all aragonitic bioclasts throughout the section were dissolved to form moldic pores, but the contribution of these secondary pore volumes to present porosity depends on the degree of infilling by later coarse cements. Porosity creation by dissolution under burial conditions (Mazzullo and Harris, 1992) appears not to have occurred to any significant extent in the Finnmark Platform cores. Instead, burial diagenesis appears to have consisted of progressive gradual porosity occlusion by growth of coarse calcite, dolomite, and anhydrite cements.

POROSITY AND BULK-ROCK ALUMINA

A broad negative correlation is apparent between the largest (>50 m; >164 ft) scale of porosity variation and both bulk-rock alumina content and gamma-ray activity in the 7128/6-1 section (Figures 4, 9A). However, poor correlation exists between porosity and alumina on a sample-by-sample basis, except that low-Al samples have a wider range of porosity and higher average and maximum porosity compared with more Al-rich carbonates (Figure 9B). Thus, higher alumina content ensures low porosity, whereas low alumina content allows but does not ensure high porosity. This relationship is defined mainly by limestones and partly dolomitized limestones but not dolostones because few dolostones in the cored intervals have Al-rich composition.

Smoothing of the alumina and porosity profiles by a moving average results in stronger negative correlation between alumina and porosity (Figure 9C). Considerable noncorrelated small-scale variability exists in alumina content and porosity, but an overall negative relationship between alumina and porosity exists over broad stratigraphic intervals. This may indicate that high abundances of aluminosilicate minerals are associated with low porosity both in the same sample volume and in nearby low-alumina beds.

Table 1. Facies Descriptions and Pore Types in Moscovian to Lower Sakmarian Cores

Facies	Name	Description	Interpretation	Stratigraphic %*	Thin-Section Porosity %*	Primary Pores %*	Moldic Pores %*	Inter-xl Pores %*
F3	bryozoan-echinoderm wackestone	bioclasts are mainly bryozoan and echinoderm fragments	open marine, near storm wave base	8				
F4	bryozoan-echinoderm grainstone and packstone	bioclasts are mainly bryozoan and echinoderm fragments	open marine, between storm and fair-weather wave base	2				
F5	fusulinid and foraminifer wackestone	biota is similar to F7, but with predominant fusulinids and few or no algae	shallow shelf, below fair-weather wave base	11	12	14	27	59
F6	buildup	fabric is dominated by plates of *Palaeoaplysina* and/or phylloid algae in micropeloidal mud matrix	shallow shelf, below fair-weather wave base	23	11	35	43	22
F7	foraminifera grainstone and packstone	allochems include small benthic foraminifera, algae, peloids, bryozoans, echinoderms, brachiopods	high-energy sand shoals	24	12	86	10	4
F8	dolomitic mudstone	fabric varies from structureless to bioturbated to thinly laminated; common anhydrite and silica nodules and varying quartz silt and sand content; biota varies from nil to fine sand-size molds	hypersaline lagoon to intertidal to sabkha	13	11	0	16	84
F9	shale and marl	varying silt and bioclast contents (nil to abundant), with biota typically including bryozoans and echinoderms	lower shoreface to offshore	4				
F10	calcareous siltstone	siliciclastic silt, commonly with bioclasts of bryozoans, echinoderms, fusulinids	lower shoreface	6				
F11	calcareous sandstone	siliciclastic sand, typically with bioclasts similar to F7 or F10 biota	nearshore marine	9	15	0	73	27
F12	anhydrite	nodular fabric with fine-felty texture	evaporative lagoon or salina	0.6				

*Stratigraphic % = percentage of the total 326 samples assigned to each facies; thin-section porosity % = estimated porosity visible in thin section (average for samples with plug porosity >10%); primary pores % = percentage of thin-section (visible) porosity that appears primary, including intergranular macropores, finer pores in areas of recrystallized but undolomitized mud matrix, and intrafossil pores; moldic pores % = percentage of thin-section (visible) porosity that appears formed by allochem dissolution; inter-xl pores % = percentage of thin-section (visible) porosity that appears intercrystalline (between dolomite crystals).

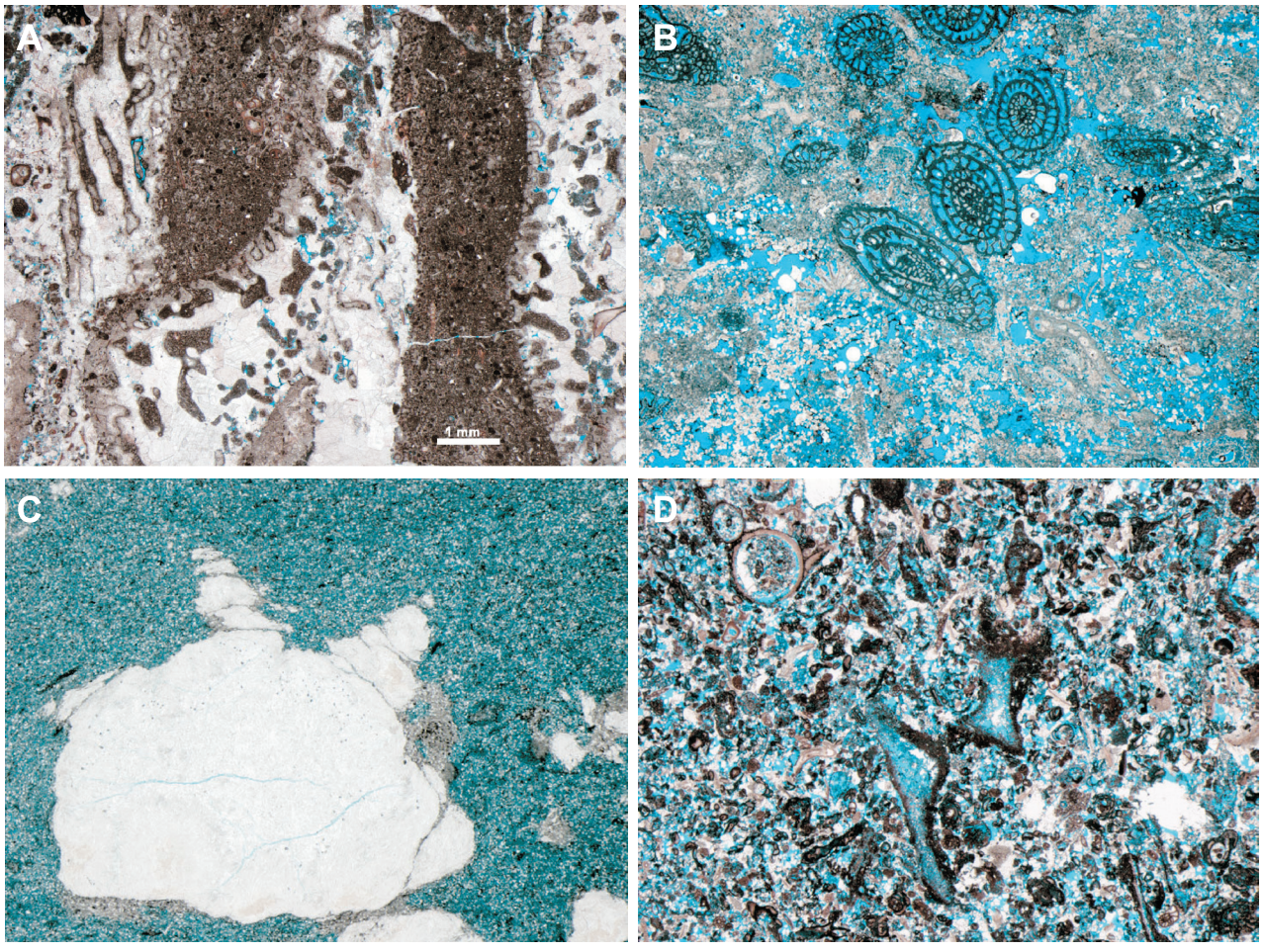

Figure 7. Photomicrographs illustrating main porosity-prone facies in Gipsdalen Group cores. Constant scale in all views. (A) Buildup facies, consisting of *Palaeoaplysina* molds and micropeloidal mud matrix (brown), which partly fills former canals in plates. The aragonite plates were dissolved and then filled with calcite cement (white), which shows increasing crystal size away from plate and canal walls. Only minor macroporosity (blue) remains uncemented. (B) Fusulinid wackestone facies, consisting of undolomitized fusulinids with high intrafossil macroporosity and dolomitized bioclast-rich matrix with both moldic and intercrystalline porosity. (C) Dolomitic mudstone facies, consisting of a microporous matrix of fine dolomite crystals with abundant quartz silt and anhydrite nodules (white areas). (D) Foraminifera grainstone and packstone facies, consisting of diverse biota with high intergranular and intrafossil porosity that has been partly filled by fine calcite cement coating bioclast, coarser mosaic calcite spar (smaller white areas), and patchy anhydrite cement (larger white areas).

Intervals having low to moderate alumina content but distinctly low porosity (<5%) are especially notable in two parts of the section. In unit L-4 and lower L-5, there is a series of five intervals, each 3–5 m (10–16 ft) thick, characterized by pronounced gamma-ray peaks and porosities mostly less than 5% (Figure 4) and interpreted as the transgressive tracts of smaller scale sequences or parasequences (Ehrenberg et al., 1998a). Porosity in these intervals has been lost by pervasive chemical compaction in fusulinid wackestones having abundant stylolitic dissolution surfaces lined with dark brown material and by heavy calcite-spar cementation in the immediately adjacent beds of other lithologies. The gamma-ray peaks corresponding with these intervals reflect high uranium contents but generally low to moderate K and Th (Ehrenberg and Svånå, 2001), suggesting that the dark brown material associated with stylolitic dissolution in the wackestones may be mainly organic matter with only subordinate clay content. Second, in upper unit L-6 and upper unit L-7, low porosities in clean (low-Al) grainstones and packstones are interpreted to be related to stylolite development along thin shaly surfaces that tend not to be included in the points sampled for bulk chemistry and which have little aggregate effect on the gamma-ray log (Figure 4). These intervals

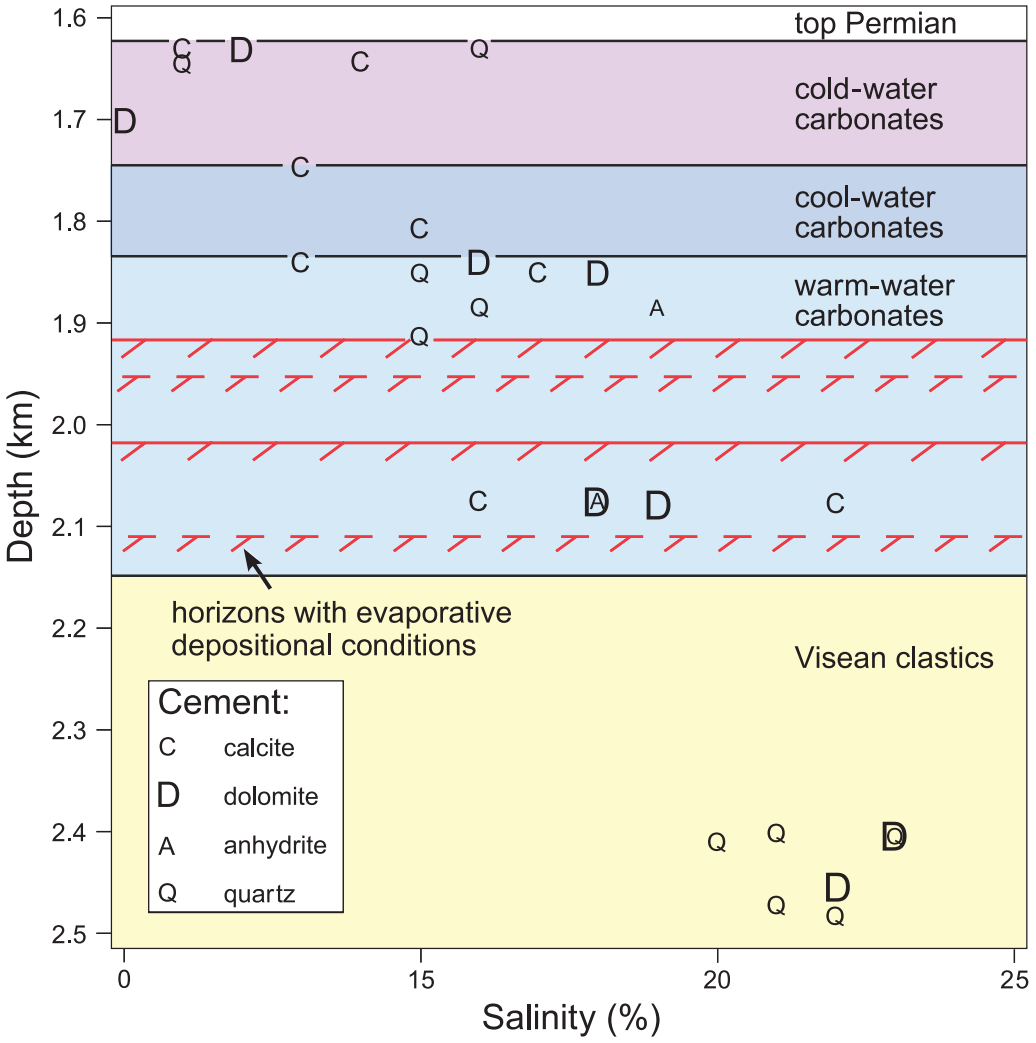

Figure 8. Depth vs. salinity (wt.% NaCl equivalent) of primary fluid inclusions in cements in upper Paleozoic strata of wells 7128/4-1 and 7128/6-1. Each point represents the average value measured for the indicated cement in one sample. Plotting symbols indicate mineral type. Cementation of these strata took place in a stratified column of hypersaline pore water. Modified from Ehrenberg et al. (2002) with permission from the Society for Sedimentary Geology.

are discussed in the following section concerning units L-6 and L-7.

The overall negative correlation between bulk alumina content and porosity (Figure 9B) is proposed to result from two related phenomena: (1) the effect of clay and mica on promoting both early mechanical compaction and subsequent chemical compaction of limestones (Weyl, 1959; Oldershaw and Scoffin, 1967; Choquette and James, 1987; Brown, 1997) and (2) cementational porosity loss sourced by dissolution along stylolites (Bathurst, 1983; Purser, 1984; Koepnick, 1985), the development of which was localized by depositional concentrations of phyllosilicate minerals. There has been much discussion about whether noncarbonate materials lining stylolites in carbonate rock are the cause or the result of dissolution (Bathurst, 1983; 1987). Nevertheless, the facilitation of stylolitic dissolution by phyllosilicate mineral surfaces is well documented for quartz grains in sandstones (Heald, 1959; Bjørkum, 1996), and there seems no reason to believe that this effect is not similarly important for carbonate minerals.

Negative correlation between bulk-rock alumina content and porosity has previously been noted for sandstone reservoirs (Ehrenberg, 1997), although this relationship may easily be obscured by grouping together samples with widely differing thermal histories. The conclusions set forward by Ehrenberg (1997) should therefore apply equally well to the carbonates of the present study as to the Brent Group sandstones of the Viking Graben.

RELATIONSHIP OF POROSITY TO FACIES AND DOLOMITIZATION

The relationship of facies to porosity is examined in Figure 10, where it is apparent that the five most abundant facies, as listed in Table 1, each contain a

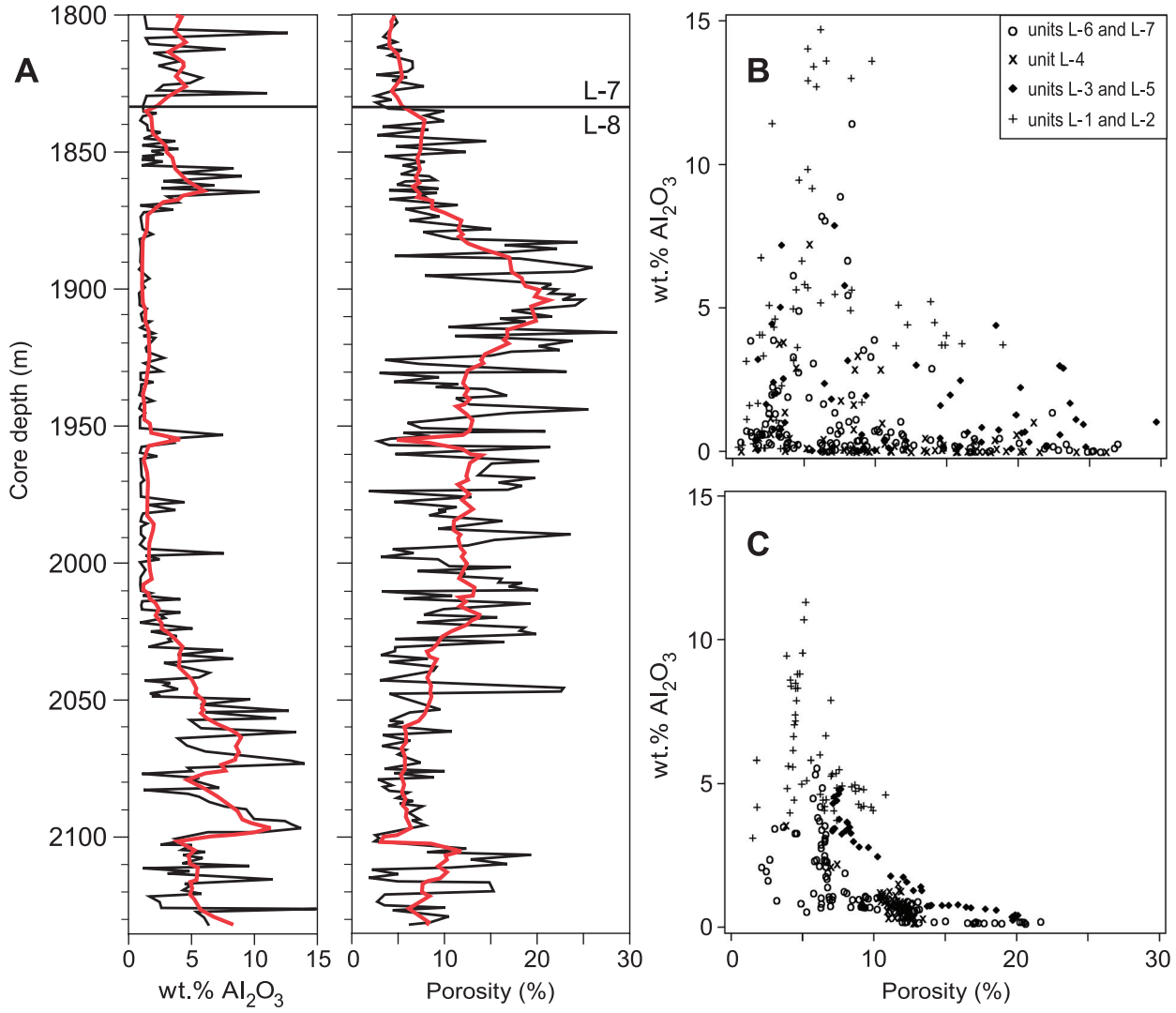

Figure 9. Relationship between bulk-rock alumina content and porosity. (A) Depth profiles of bulk chemical analyses and plug porosity values for corresponding plugs. Red curves are 25 m (82 ft) running averages of individual analyses shown by black curves. (B) Individual bulk chemical analyses vs. plug porosity values from the same depth. Plotting symbol indicates stratigraphic interval. (C) The 25-m (82-ft) running average of data in (B). Overall negative correlation between alumina and porosity reflects the influence of phyllosilicate minerals on promoting chemical compaction and associated calcite cementation.

wide range of low to high porosity. The other facies (F3, F4, F9, F10, and F12) are not prone to include high porosity values. Figure 10 also shows that certain facies are porosity prone in particular units but not in other intervals.

Despite poor overall correlation between porosity and dolomitization (Figure 11), comparison of the depth profiles of porosity and dolomitization index in Figure 4 reveals that strong correlation exists in certain stratigraphic intervals. For example, in unit L-1 (Figure 4), limestones are tightly cemented (<5% porosity), mainly by coarse calcite spar, whereas adjacent beds of dolomitic sandstone to mudstone have little calcite spar and high porosity. This pattern is consistent with purely local derivation of the late calcite cement from stylolites that developed preferentially in the limestone beds. Units L-3 and L-5 also show overall porosity-dolomite correlation, whereas units L-4 and L-6 do not. These differences reflect the different facies proportions in different stratigraphic units and the different factors controlling porosity differentiation in different facies.

Because the effect of dolomitization on porosity evolution seems to vary with stratigraphic position, it is necessary to examine facies and dolomitization together in specific stratigraphic units to determine the nature of possible relationships. Four facies categories

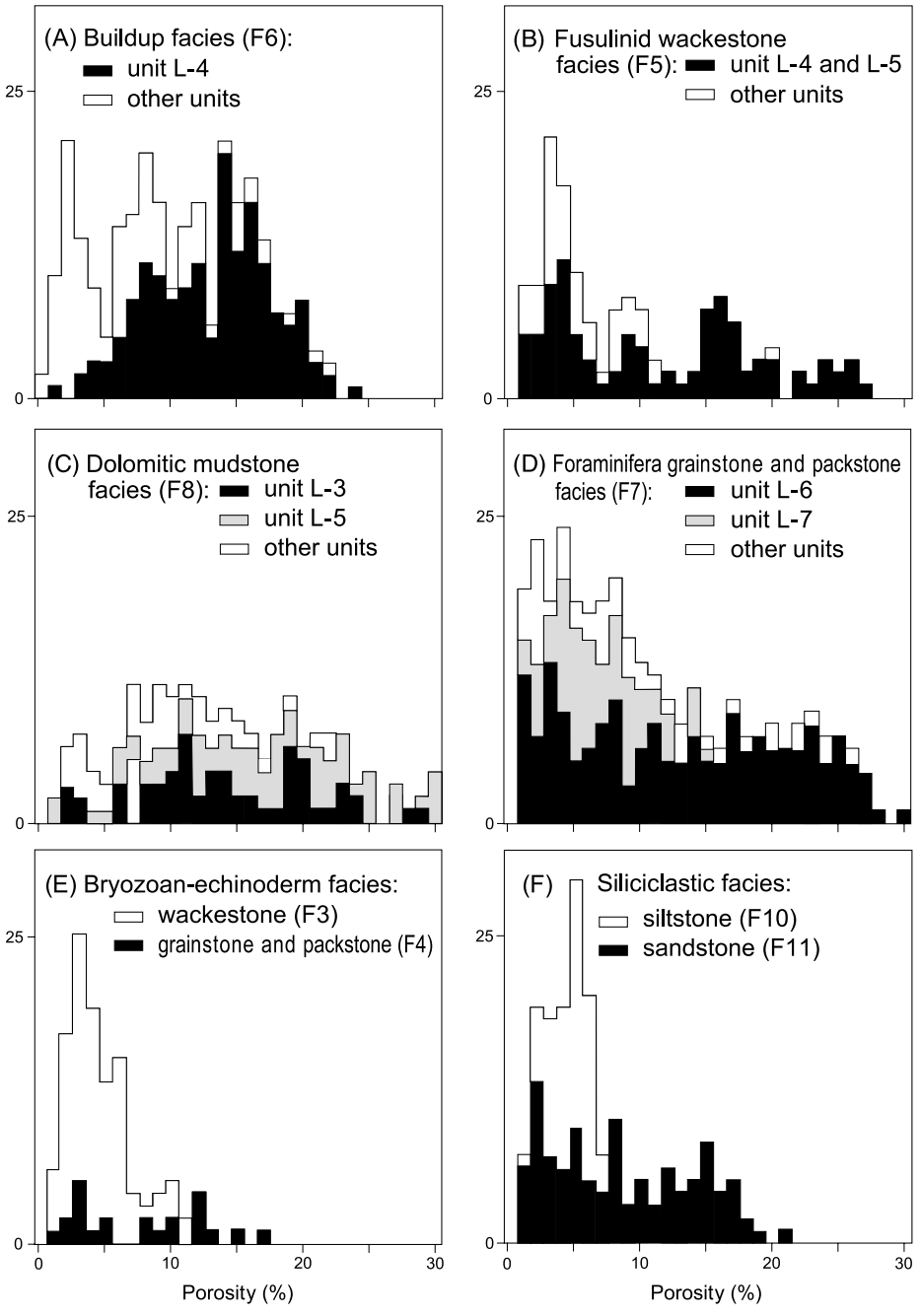

Figure 10. Frequency distributions of porosity in different facies categories comprising the Gipsdalen Group in cores from wells 7128/4-1 and 7128/6-1. Plugs were assigned to facies based on core descriptions and thin sections (1-m [3.3-ft] spacing through most intervals). Bar patterns distinguish different stratigraphic units in (A–D) and different facies in (E–F). "Other units" in (A–D) refer to units (L-1 to L-7) not specified by filled patterns in each plot. Some facies have wider porosity variation than others, and certain facies are more porosity prone in particular stratigraphic intervals.

were examined in particular detail to determine the causes of porosity variation:

- *Palaeoaplysina*-phylloid-algae buildups (F6), which dominate in unit L-4
- fusulinid wackestones (F5), abundant in units L-4 and L-5
- dolomitic mudstones (F8), dominant in units L-3 and L-5
- foraminifera grainstone and packstones (F7), dominant in units L-6 and L-7

Buildup Facies (F6) of Unit L-4

Palaeoaplysina-phylloid-algae buildups (F6) include many porosity values greater than 10% in unit L-4 but have mostly less than 10% porosity in other units (Figure 10A). Throughout the succession, this facies is characteristic

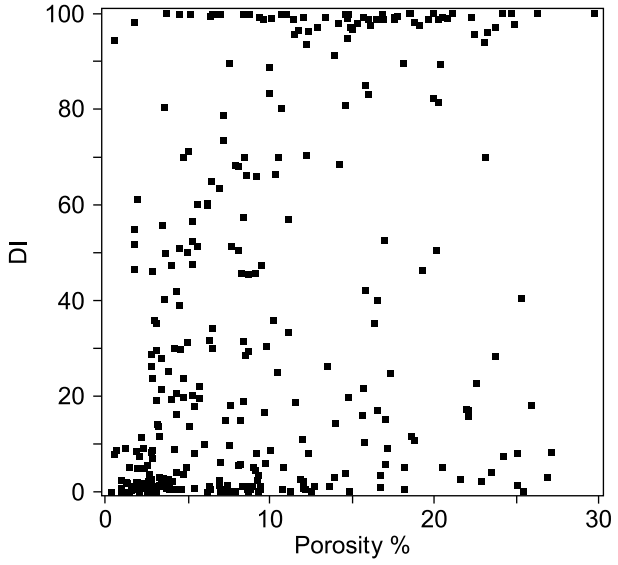

Figure 11. Dolomitization index (DI = 100 × dolomite/total carbonate, mostly determined by bulk x-ray diffraction) vs. porosity in the Gipsdalen Group of wells 7128/4-1 and 7128/6-1. Samples are mainly at constant 1-m (3.3-ft) spacing and should therefore be roughly representative of lithologic proportions present. No linear correlation of porosity with dolomitization exists when facies are grouped together, although porosity distribution is focused at low values in the limestones.

of the regressive (highstand) portions of depositional cycles. Petrographic comparisons were made between F6 samples from unit L-4 with contrasting high porosity vs. low porosity. Distinction was also made between little-dolomitized vs. extensively dolomitized intervals.

Interestingly, there is no apparent difference in overall porosity distribution between dolomitized and undolomitized buildups in unit L-4 (Figure 12A). In little-dolomitized buildups with high porosity, coarse calcite spar tends to be scarce or only modestly developed. In contrast, low-porosity samples tend to show extensive infilling of *Palaeoaplysina* and phylloid molds and other fossil cavities by coarse calcite spar (Figure 7A). For the extensively dolomitized buildups, high-porosity samples tend to have abundant visible porosity in the form of both molds and intercrystalline matrix porosity, whereas low-porosity samples have lost porosity mainly by plugging of molds and intercrystalline pores by anhydrite or by coarsely crystalline dolomite cement. Thus, high porosity in buildup facies is associated with abundant open moldic pores, mainly formed by dissolution of aragonitic bioclasts, whether the buildups are dolomitized or not. Low porosity most commonly reflects infilling of molds and fossil chambers by late calcite spar in the little-dolomitized buildups or by coarse anhydrite and dolomite cements in extensively dolomitized buildups.

Fusulinid Wackestone (F5) of Units L-4 and L-5

Facies F5 includes porosity values greater than 10% in units L-4 and L-5 but has mostly less than 10% porosity in other units (Figure 10B). A general correlation of low porosity with less dolomitization in facies F5 exists, but completely dolomitized F5 samples still show a wide porosity range (Figure 12B). F5 samples with greater than 10% porosity tend to contain both intercrystalline macroporosity in dolomitized matrix areas and intrafossil macroporosity in bioclasts that have resisted dolomitization (Figure 7B). These bioclasts appear to be represented by molds in completely dolomitized F5 samples. Tight F5 samples (<5% porosity) typically have matrix areas that have low porosity because of both compaction and calcite cementation. This facies is characteristic of both transgressive and regressive portions of depositional cycles, with lowest porosities typically found in the former.

Dolomitic Mudstone (F8) of Units L-3 and L-5

Porosity varies widely and shows a thinly layered pattern of vertical variation (Figures 4, 10C). These variably silty mudstones to bioclast-poor wackestones are mostly replaced by finely crystalline (2–20-μm) dolomite (Figure 7C). They are interpreted as having been deposited in low-accommodation lagoonal, intertidal, to sabkha settings and comprise numerous thin depositional cycles, mostly 0.1–1 m (0.3–3.3 ft) thick. Only sparse examples have similar appearance but low dolomite content (Figure 12C).

In general, high porosities in F8 samples reflect high intercrystalline matrix porosity combined with varying contributions of microvuggy (moldic) porosity. Although a few low-porosity plugs are located in anhydrite and silica nodules, most low-porosity values reflect low intercrystalline porosity of tightly packed microdolomite matrix. Thus, the jagged profile of frequent, wide porosity variation in the dolomitic mudstones reflects the thinly bedded character of these shallow-water deposits, with apparent cyclic alteration of high- and low-porosity layers. Although the underlying causes of porosity preservation and occlusion in these beds are obscure, it may be speculated based on the microvuggy fabric and euhedral (microsucrosic) dolomite texture characteristic of the porous mudstones

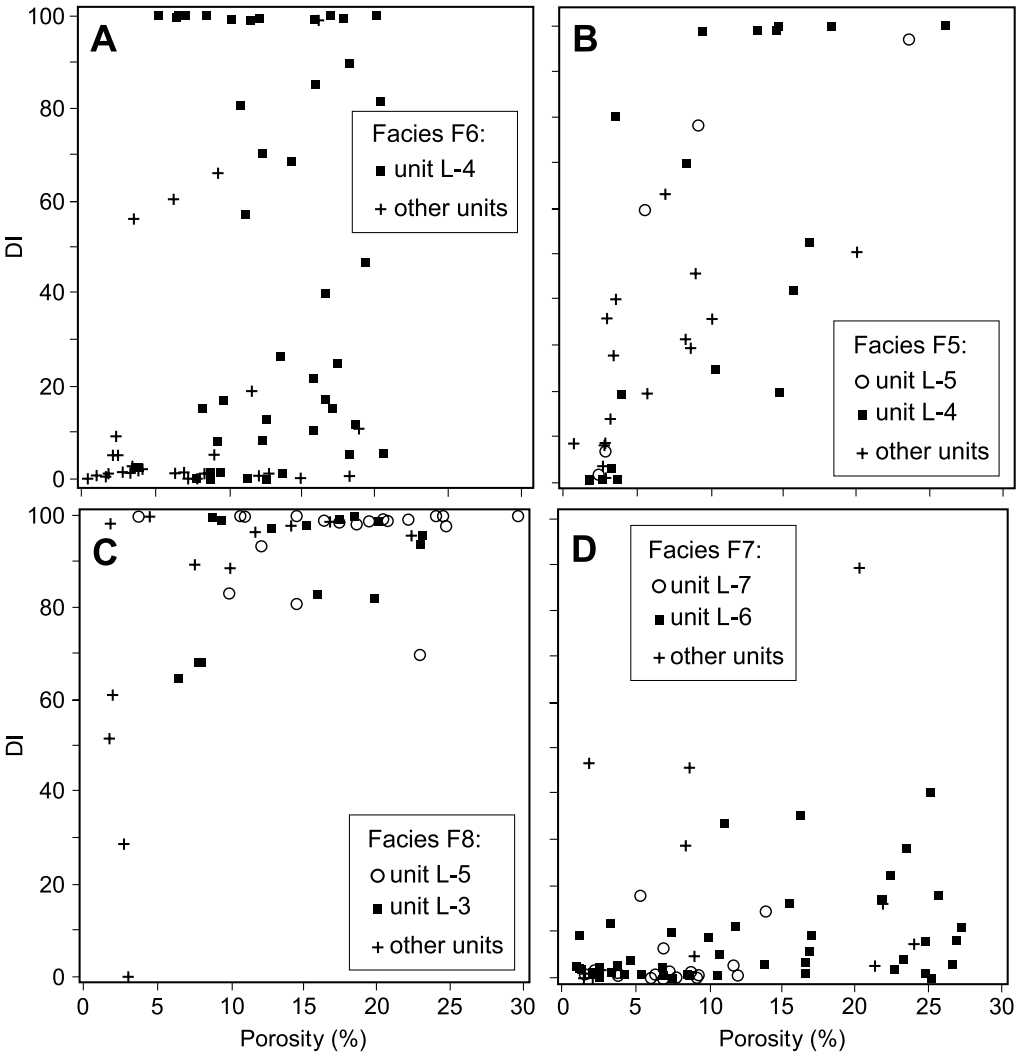

Figure 12. Dolomitization index (DI = 100 × dolomite/total carbonate, mostly determined by bulk x-ray diffraction) vs. porosity in samples from the four main porosity-prone facies comprising the Gipsdalen Group of wells 7128/4-1 and 7128/6-1. Plotting symbols indicate samples from particular stratigraphic units. "Other units" refer to units (L-1 to L-7) not specified by squares or circles in each plot.

and wackestones that porosity has been enhanced by dissolution of remaining calcite mud and bioclasts after growth of a supporting framework of fine dolomite crystals (Murray, 1960; Dawans and Swart, 1988).

Bulk-carbonate oxygen isotopic values of the dolomudstones in units L-5 and upper L-3 are about −3 to −5 ‰ Peedee belemnite (PDB), which is distinctly lower than expected for dolomite formed in equilibrium with Lower Permian seawater and thus possibly indicative of pervasive meteoric water influence (Ehrenberg et al., 2002). Dolomitization and leaching of age-equivalent carbonates on Bjørnøya (Figure 1) have previously been linked with alternating hypersaline and meteoric water compositions (Folk and Siedleka, 1974; Stemmerik and Larssen, 1993). Selective early dissolution of calcite from partly dolomitized L-3 and L-5 mudstones and wackestones may have also been promoted by eogenetic oxidation of organic matter deposited in the shallow lagoonal and peritidal setting inferred for these beds.

Foraminifera Grainstone and Packstone (F7) of Units L-6 and L-7

Facies F7 includes many porosity values of greater than 10% in unit L-6 and in some other units (mainly L-4 and L-5) but has mostly less than 10% porosity in unit L-7 (Figure 10D). From units L-6 and L-7, 13 samples with the highest porosity (>20%) were compared with 20 samples with the lowest porosity (<5%). These rocks are undolomitized or have relatively minor development of microdolomite rhombs in their recrystallized mud matrix (Figure 12D). The high-porosity samples are characterized by abundant primary intergranular and intrafossil porosity (Figure 7D). In addition, many of the porous samples are packstones having a highly porous matrix of calcite microspar with subordinate fine dolomite cement. The low-porosity samples show extensive occlusion of the same pore types that characterize the high-porosity samples by fine to coarse calcite-spar cement.

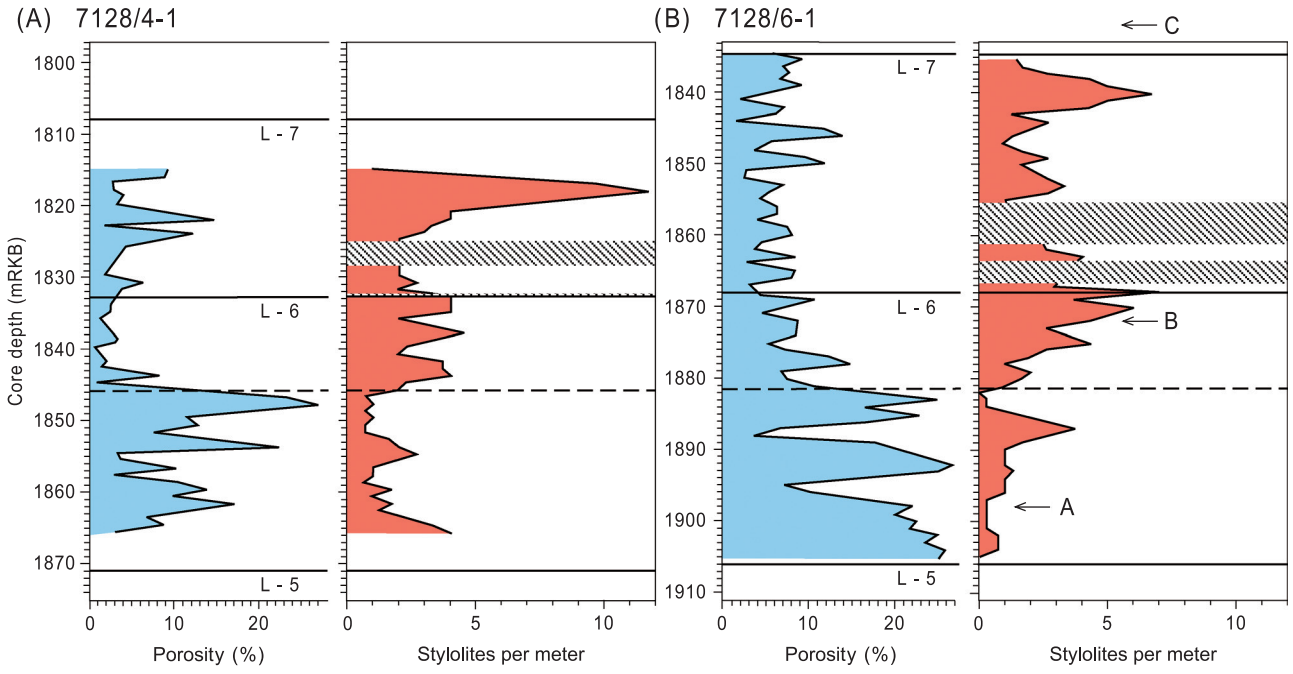

Figure 13. Profiles of porosity and stylolite frequency through units L-6 and L-7 in wells 7128/4-1 and 7128/6-1. Counts of number of stylolites in each meter of core have been smoothed by averaging every 3 m (10 ft). Intervals consisting of shale and shaly wackestone (diagonal pattern) are excluded from this count because they lack macroscale stylolites. These shaly intervals, however, show petrographic evidence of extensive microstylolitic dissolution throughout. Horizontal lines indicate boundaries of lithostratigraphic units. This comparison shows that the point of abrupt upward porosity decrease in each well (dashed line) is laterally correlative and corresponds with an upward increase in overall stylolite frequency. Letters with arrows in (B) indicate locations of core photographs in Figure 14. Location C is within the lower part of lithostratigraphic unit L-8. Modified from Ehrenberg et al. (1998b) with permission from the Geological Society of Norway.

Thus, the wide porosity variation in units L-6 and L-7 appears to be mainly a function of the degree to which primary porosity has been infilled by calcite cement. One can also point to additional factors involved in the development of the higher porosity zones, such as the removal of aragonitic skeletal material by early leaching, the near absence of early marine fibrous cements, and the lack of anhydrite plugging, but these are factors that are common to the low-porosity zones as well. Another difference is the modest amounts (mostly <10%) of fine dolomite rhombs in F7 samples with higher porosity (Figure 12D). The timing of this dolomite is uncertain; if it was early, it may have formed in association with dissolution of mud matrix, but if it was late, it may simply reflect the preferred access of dolomitizing fluids to the more permeable beds not already occluded by calcite cement.

Units L-6 and L-7 were cored in both of the wells studied. The porosity profile of this interval shows similar characteristics in both wells (Figure 13), in that the lower part of the interval contains high-porosity zones, whereas the upper part has only low to moderate porosity. The point above which high porosities (>10%) become sparse is very distinct (1846 m in well 7128/4-1 and 1881 m in well 7128/6-1). This may represent a correlative stratigraphic horizon above which there was a change in depositional or early diagenetic conditions significant for porosity development. Again, the comparison of high-porosity vs. low-porosity samples above and below this horizon shows that the main reason for the difference in porosity is the abundance of coarse, blocky calcite cement, whereas depositional textures and biota are similar.

The underlying cause of the above differences in calcite-spar abundance is suspected to be related to development of stylolites, dissolution along which is envisioned to be the main source for the coarse calcite spar in these rocks. Correlation between stylolite occurrence and cementational porosity loss in limestones has been widely observed previously (Harms and Choquette, 1965; Dunnington, 1967; Muin and Hastowidodo, 1982; Purser, 1984; Choquette and James, 1987). A meter-by-meter count of the number of

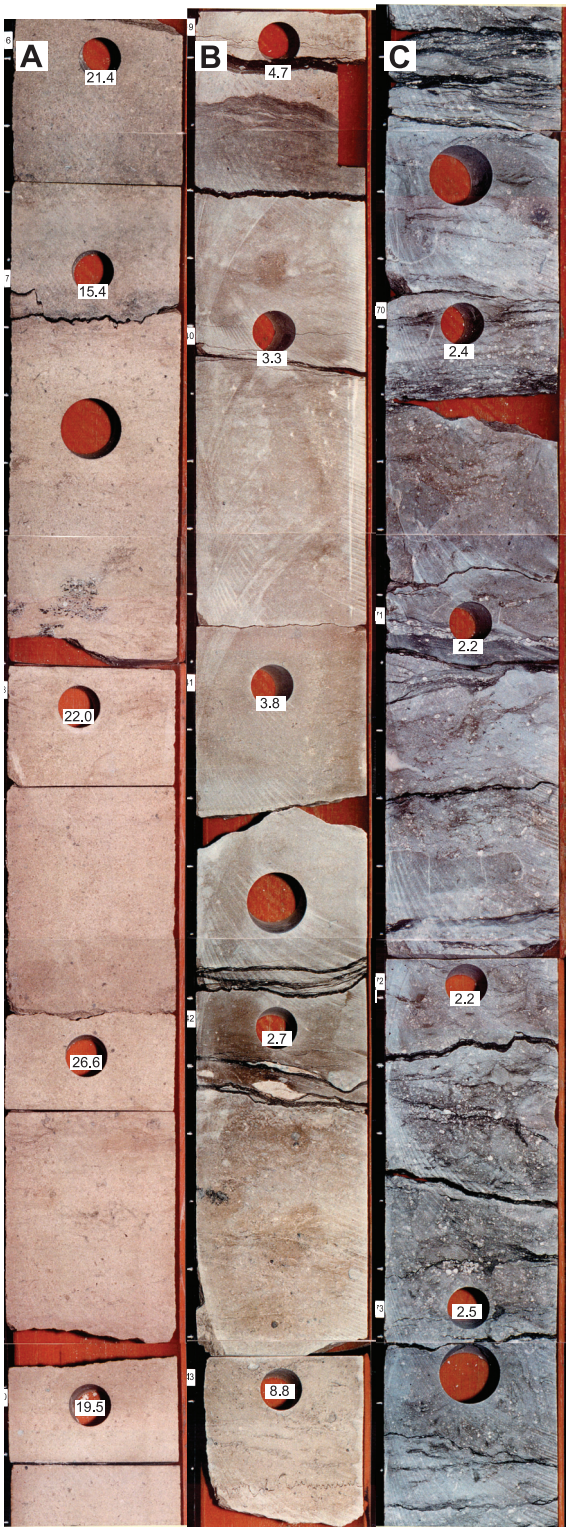

Figure 14. Photos of 7128/6-1 cores illustrating different stylolite frequencies characteristic of different intervals. Approximate locations are indicated in Figure 13B. Core width is 12.8 cm (5.04 in.). Labels give porosity values corresponding to each plug location. (A) 1897.6–1898.3 m (lower unit L-6); (B) 1871.4–1872.2 m (upper unit L-6); and (C) 1828.7–1829.5 m (lowermost unit L-8).

easily visible stylolites on the core surface in units L-6 and L-7 indicates overall greater frequency in the upper (lower porosity) zone in each well (Figures 13, 14). This upper zone also includes two beds of carbonate-rich shale to shaly wackestone that have undergone extensive chemical dissolution during burial, as evidenced by pervasive dissolution textures where bioclasts are truncated against tiny clay seams. Unit L-7 and the upper part of unit L-6 are locally cut by veins of coarse calcite spar, possibly attesting to the export of calcite-saturated waters. Stable isotope analyses of two such veins (1837.5 m in well 7128/4-1 and 1842.6 m in well 7128/6-1) yielded values of $\delta^{18}O = -6.0$ to -10.9 ‰ PDB and $\delta^{13}C = 4.1$ to 5.0 ‰ PDB, which are similar to the range of coarse calcite cements from this interval (Ehrenberg et al., 2002).

Porosity loss throughout the overlying unit L-8 (97 m [318 ft] thick, consisting mainly of bryozoan-echinoderm grainstone to wackestone of facies F4 and F3) is also believed to reflect the presence of closely spaced, clay-lined stylolites, here having even higher frequency than in unit L-7 (Figure 14C). Extensive calcite cementation in facies F4 was also facilitated by the abundance of echinoderm fragments, which provide sites for syntaxial cement overgrowth.

SELECTIVE POROSITY LOSS IN LIMESTONES

Limestone and dolostone in the Finnmark Platform strata have very different porosity frequency distributions (Figure 15). Limestones have lower average porosity (8.2%) with positively skewed distribution, whereas dolostones have higher average porosity (14.4%) with symmetric distribution. Partially dolomitized limestones resemble the limestones in having low average porosity (8.2%) and positive skewness but are similar to the dolostones in having a low proportion of samples with porosity less than 5%. The limestone characteristics have important implications for reservoir modeling of fluid flow because the low-porosity limestones represent a series of barriers to vertical and perhaps also lateral flow, which are distributed according to both parasequence- and sequence-layering scales (Figures 4, 9A).

As discussed above, porosities below 5% in the limestone distribution (Figure 15A) seem to result from different processes in different lithologies. Many of these low-porosity samples are grainstones, packstones, and buildups where low porosity results from heavy cementation by coarse calcite spar (41% of the

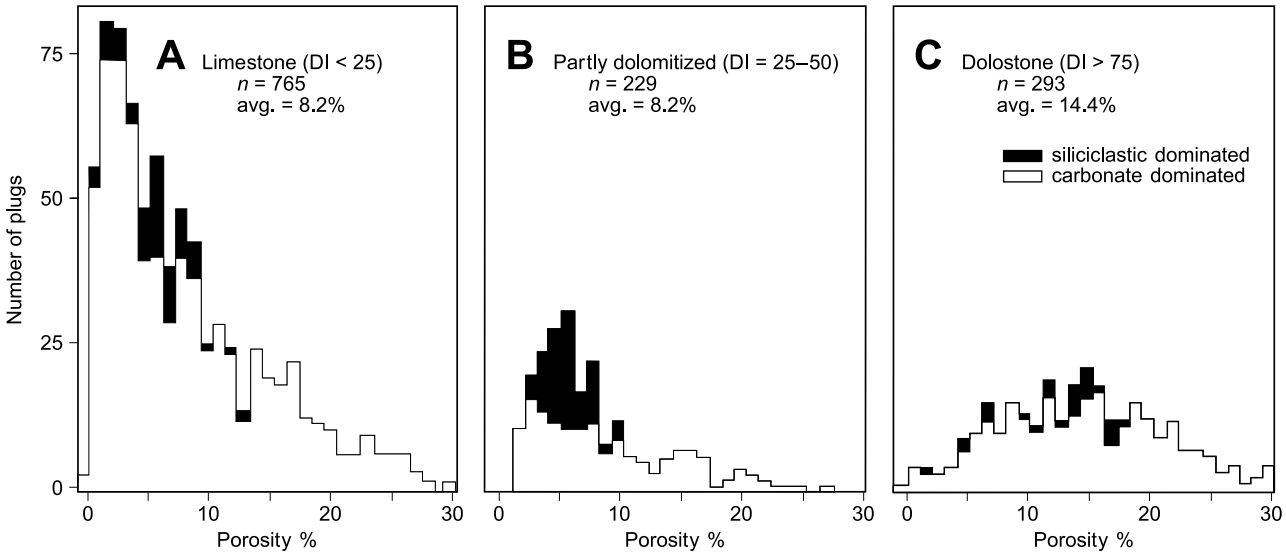

Figure 15. Frequency distributions of porosity in limestones, partly dolomitized limestones, and dolostones of the Gipsdalen Group (units L-1 to L-7) in cores from wells 7128/4-1 and 7128/6-1. Approximately every third plug sample was assigned a dolomitization index (DI = 100 × dolomite/total carbonate) based on bulk x-ray diffraction or petrographic analysis (1-m [3.3-ft] spacing through most intervals). Intervening plugs were then assigned an approximate DI range by interpolation between analyzed samples, with guidance from core descriptions. Filled pattern indicates more than 50% siliciclastic content (estimated for the fixed-interval samples from bulk chemical analysis and interpolated for intervening plugs based on core description). This comparison shows that limestones have vastly different proportions of low, moderate, and high porosity values compared with interlayered dolostones, supporting the view that dolomitization slows porosity loss attending burial.

103 plugs with porosity <5% and also represented by thin sections). Other low-porosity limestones are wackestones and mudstones, where porosity loss has occurred by compaction and cementation of the mud matrix (32% of the low-porosity thin sections). Calcite cementation is also the main cause of porosity loss in calcareous siltstones and calcareous sandstones of units L-1 and L-2 (22% of the low-porosity thin sections). Limestones of unit L-8 (not included in Figure 15) have consistently low porosity (1–4%) caused mainly by extensive calcite cementation that may be related to closely spaced stylolites and abundant echinoderm grains (sites for syntaxial calcite cement growth).

The higher average porosity and the normal porosity distribution of dolostones reflect their minor calcite-spar cementation combined with early replacement of mud matrix by microporous dolomite. The latter process apparently hinders matrix compaction and cementation. Lesser calcite cementation in dolostones may stem, in large part, from the lesser propensity for stylolite development in dolostone intervals, as observed in the present cores and suggested by previous reports (Choquette and Steinen, 1980; Schofield, 1984; Railsback, 1993; Purser et al., 1994; Amthor et al., 1994; Brown, 1997). The spatial association between stylolite occurrence and calcite cementation in the same beds (also noted by Wong and Oldershaw, 1981) suggests that the solutes released by stylolitization tend not to be exported far from their point of origin, implying that solute supply, instead of transport or precipitation, may be the rate-limiting step for limestone cementation at burial temperatures (Oelkers et al., 1996).

INFLUENCE OF STRATIGRAPHIC POSITION ON POROSITY

In common with the sedimentologic cycle hierarchy, patterns of vertical porosity variation in wells 7128/4-1 and 7128/6-1 have both smaller scale and larger scale components of variation. At approximately the same spatial magnitude as the facies variations defining the sedimentologic cycles or smaller sequences, wide porosity fluctuations occur on the meter to decimeter scale and commonly coincide with cycle boundaries (Figure 4). The porosity profile also shows overall trends distinctive to each of the four major (7–9 m.y.) sequences. On the largest (second-order) scale, the 7128/6-1 porosity profile shows a pronounced trend

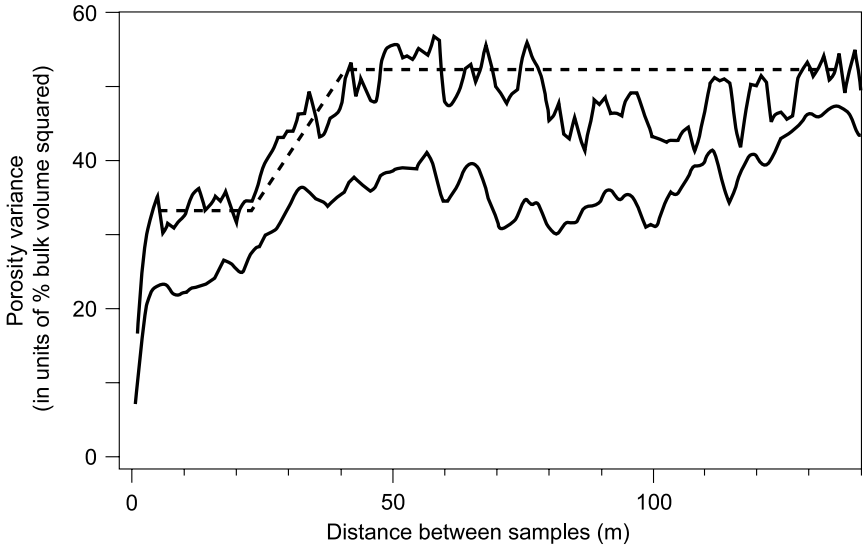

Figure 16. Semivariograms of porosity in the Gipsdalen Group of well 7128/6-1, based on plug data (upper curve) and wire-line–log data (lower curve). See Lucia (1999) for explanation of how variograms work. Sills (plateaus) at roughly 5–25- and more than 40-m spacing (dashed line) reflect parasequence and sequence scales of layering.

of upward porosity increase from the base of the carbonate-platform succession to a maximum in unit L-6, followed by a relatively abrupt decrease in the upper part of unit L-6 (Figures 4, 13).

Semivariograms for plug and log data show that porosity has two main scales of variance in the vertical dimension (Figure 16). More than half of the total variability is contained in the parasequences (0–5-m [0–16-ft] scale), indicating that porosity contrasts in cycles are greater than between cycles. Following a sill from 5- to 25-m scale, variance then increases from 25 to 40 m, somewhat less than the 50–110-m scale of the major sequences.

The above patterns have fundamental implications concerning the processes controlling the occurrence of higher porosity in these carbonates. The dominance of intracycle porosity variation implies that the differences in lithology and eogenetic diagenesis defining the sedimentologic cycles are also of primary importance in determining porosity evolution. This link is confirmed by detailed comparisons between core descriptions and the plug porosity profile (Ehrenberg et al., 1998b). Superimposed on this extreme, fine-scale heterogeneity is a larger scale (roughly 30–60 m [100–200 ft]) pattern where intervals containing frequent high-porosity peaks alternate with intervals containing fewer or no high-porosity values (Figure 9A). This larger scale of porosity variation is linked to the systems tracts comprising the lower order sequences.

The position of the overall porosity maximum in 7128/6-1 section above (at approximately 1900-m [3200-ft] depth), instead of immediately below, the second-order sequence boundary (Figure 4) militates against karstic dissolution as a principal means of creating high porosity in these strata. In contrast to the Finnmark Platform, however, widespread collapse features caused by meteoric dissolution of underlying evaporate beds (not present in the inner Finnmark Platform) are observed in stratigraphically equivalent carbonates of Spitsbergen and in the subsurface of the Loppa high (Figure 1) (Eliassen and Talbot, 2001).

The large-scale correlation between porosity and the platform's stratigraphic evolution is believed to result from the combined effects of phyllosilicate distribution, depositional texture (facies), dolomitization, and stratigraphically localized calcium-sulfate cementation:

- The early platform stage of mixed siliciclastic-carbonate deposition (units L-1 to lower L-3) has generally low porosity because of extensive chemical compaction in aluminous beds and associated cementation of interlayered clean carbonate beds.
- The following siliciclastic-poor stage of platform evolution shows upward-increasing porosity because agggradation of muddy buildups and wackestones (unit L-4) was followed by progradation of a more proximal facies belt of thinly bedded dolomitic mudstones (unit L-5), where high porosity reflects early replacement of mud matrix by finely crystalline dolomite, possibly combined with leaching of calcite from partly dolomitized beds.
- Maximum porosity development occurs in the overlying, little-dolomitized grain-shoal facies belt (unit L-6), where high primary macroporosity (intergranular and intrafossil pores) is favorably combined with

the low frequency of stylolite-prone shaly layers. A similar but thinner grainstone and packstone interval is developed in lower unit L-5 (Figure 4), but here porosities were extensively plugged by coarse anhydrite cement, possibly because of refluxing of brines related to the restricted lagoonal and sabkha setting of the overlying dolomitic mudstones.

- Further backstepping toward the top of the photozoan platform section (unit L-7) is expressed by porosity decrease because lower energy depositional conditions favored more frequent occurrence of stylolite-prone shaly laminations, resulting in extensive calcite cementation of the high depositional to moldic macroporosity in grain-shoal and buildup facies.

HYPERSALINE WATER COLUMN AND POROSITY PRESERVATION

Fluid-inclusion data (Figure 8) show evidence for a stratified column of hypersaline pore water with salinity increasing from near gypsum saturation (12 wt.% NaCl equivalent) in Upper Permian strata to somewhat below halite saturation (26.5 wt.% at 30°C) in the Visean sandstones overlying the metasedimentary basement. The lower part of this trend (downward from the lower Sakmarian carbonates of unit L-7) could have been produced by a series of brine-reflux events occasioned by hypersaline conditions at various stages of the Upper Carboniferous–Lower Permian depositional history. Reflux involving the highest salinity (densest) brine compositions would have penetrated deepest, displacing the fresh connate waters originally present in the fluvial sandstones at the base of the section. Development of the upper part of the trend in Figure 8 (overlying unit L-7) must have involved admixture of older brines because hypersaline conditions are believed to have permanently ceased throughout the Barents Sea region in the middle Sakmarian (lower Wolfcampian), such that units L-8 and L-9 were deposited with entirely normal-marine pore waters. Mixing probably occurred because of compaction of underlying strata, producing both upward and southward movement of hypersaline water that both displaced and mixed with overlying waters of normal-marine salinity. Dewatering of the abundant shaly beds in the Upper Permian unit L-9 may also be an important factor.

Despite the above indications of displacement of original pore waters both below and above the photozoan carbonate section, the trend of density stratification inferred from Figure 8 suggests a situation of long-term hydrodynamic stability and, thus, immobility of the pore-water column. This stability would tend to enforce an overall closed diagenetic system, allowing neither convective circulation nor lateral penetration meteoric waters derived from land areas to the south. This stable and stagnant hypersaline pore water may be identified as an important general or background factor favoring porosity preservation in the present carbonates, in marked contrast to cases of extensive cementational porosity loss in carbonate platforms with open hydrodynamic systems involving large fluxes of low-salinity pore waters (Meyers, 1978; Grover and Read, 1983; Emery et al. 1988; Moore, 2001).

CONCLUSIONS

Upper Carboniferous–Lower Permian strata of the Finnmark carbonate platform contain high porosities despite maximum burial temperatures exceeding 90°C and the absence of present or past petroleum charge that could have inhibited cementation. Pore types vary widely in different lithologies but are interpreted as consisting mainly of primary (intergranular and intrafossil) pores and secondary (moldic and intercrystalline) pores that likely formed during shallow (eogenetic) diagenesis. Burial diagenetic modification appears to have involved the progressive reduction of this porosity by gradual growth of coarser cement crystals. Understanding the stratigraphic distribution of porosity therefore requires analysis of the processes favoring preservation as opposed to occlusion of porosity already present at the onset of burial below the first few hundred meters depth.

Dolomitization appears necessary for high porosity in mudstone and wackestone facies, but high porosity in grain-dominated and buildup facies is mainly dependent on paucity of burial cements. Although anhydrite and coarse dolomite are locally important, the most important burial cement is calcite, which was sourced by chemical compaction localized by phyllosilicate minerals in nearby beds. Correlation of maximum porosity development with the second-order turnaround of the platform's sequence-stratigraphic evolution is therefore explained in terms of the combined influences of (1) early dolomitization and dissolution of shallow-water mudstones and wackestones deposited as the most proximal regressive facies belt and (2) preservation

Table 2. Factors Favorable for Porosity in the Finnmark Carbonate Platform*

Abundant primary intergranular and intrafossil porosity in grain-dominated facies
Meteoric leaching of aragonitic bioclasts in buildup facies
Early dolomitization of shallow-water, muddy facies, possibly combined with early dissolution related to alternating hypersaline and freshwater conditions in partially restricted, inner shelf settings
Low frequency of clay-rich surfaces and beds prone to initiation of chemical compaction at burial temperatures
Stratigraphic position near (above and below) second-order turnaround from overall regressive to transgressive system
Photozoan biotic assemblage, as opposed to a heterozoan assemblage with abundant echinoderm fragments (sites for syntaxial calcite cement growth) and associated depositional conditions forming frequent shaly laminations (localizing stylolitic dissolution to supply cement growth)
Early emplacement of immobile pore water (stratified hypersaline brine column)

*Factors not important in this example: early petroleum emplacement; karsting and collapse features; late burial dissolution.

of primary porosity caused by low aluminosilicate content in grain shoals deposited just after the turnaround. An additional porosity-favorable factor was the early emplacement of a stratified column of hypersaline pore water, which favored closed-system behavior during subsequent burial.

These conclusions do not provide a quantitative methodology for carbonate porosity prediction, but nevertheless allow recognition of an assemblage of key porosity-controlling factors (Table 2) whose relative magnitudes can be appreciated by reference to the porosity values of the present example. This example should be of significance to carbonate reservoir evaluation elsewhere, to the extent that the factors listed in Table 2 represent physical processes operating during carbonate platform growth and diagenesis. It is important to note, however, that the present example is a particular type of carbonate platform deposited in an arid climate, with variable siliciclastic influx, consisting of diverse warm-water biota, nearly devoid of ooids and other nonskeletal allochems, and having low content of fibrous marine cements. Variation on these characteristics may result in differing importance of porosity controls.

The function of phyllosilicate minerals in facilitating stylolitic dissolution and associated cement precipitation is a fundamental similarity between carbonate and siliciclastic burial diagenesis that may have potential for calibration as a predictive tool. The contrasting porosity frequency distributions of limestones and dolostones in the present example may be a general characteristic of photozoan-assemblage carbonate reservoirs, insofar as similar relationships are also observed in cyclic, warm-water carbonate successions elsewhere (Ehrenberg et al., 2004). In any case, the low end of the limestone porosity distribution appears to represent a hierarchy of stratified barriers to fluid flow (tight limestone intervals) that are interpreted to form mainly by calcite cementation attending chemical compaction. This burial diagenetic generation of flow barriers may be a fundamental difference between carbonates and siliciclastic reservoirs, where barriers are generally formed by fine-grained, clay-rich layers that exist from the time of deposition onward (Ehrenberg et al., 1992; Olaussen et al., 1992).

REFERENCES CITED

Amthor, J. E., E. W. Mountjoy, and H. G. Machel, 1994, Regional-scale porosity and permeability variations in Upper Devonian Leduc buildups: Implications for reservoir development and prediction in carbonates: AAPG Bulletin, v. 78, p. 1541–1559.

Bathurst, R. G. C., 1983, The integration of pressure solution with mechanical compaction and cementation, *in* Stylolites and associated phenomena: Relevance to hydrocarbon reservoirs: Abu Dhabi National Reservoir Research Foundation Special Publication, p. 41–55.

Bathurst, R. G. C., 1987, Diagenetically enhanced bedding in argillaceous platform limestones: Stratified cementation and selective compaction: Sedimentology, v. 34, p. 749–778.

Beauchamp, B., and A. Desrochers, 1997, Permian warm- to very cold-water carbonates and cherts in northwest Pangea, *in* N. P. James and J. A. D. Clarke, eds., Cool-water carbonates: SEPM Special Publication 56, p. 327–347.

Bjørkum, P. A., 1996, How important is pressure in causing dissolution of quartz in sandstones?: Journal of Sedimentary Research, v. 66, p. 147–154.

Brown, A., 1997, Porosity variation in carbonates as a function of depth: Mississippian Madison Group, Williston basin, *in* J. A. Kupecz, J. Gluyas, and S. Bloch, eds., Reservoir quality prediction in sandstones and carbonates: AAPG Memoir 69, p. 29–46.

Budd, D. A., A. H. Saller, and P. M. Harris, 1995, Unconformities and porosity in carbonate strata: AAPG Memoir 63, 313 p.

Bugge, T., G. Mangerud, G. Elvebakk, A. Mørk, I. Nilsson, S. Fanavoll, and J. O. Vigran, 1995, The upper Palaeozoic succession on the

Finnmark Platform, Barents Sea: Norsk Geologisk Tidsskrift, v. 75, p. 3–30.
Cecchi, M., 1993, Carbonate sequence stratigraphy: Application to determination of play-models in the upper Paleozoic succession of the Barents Sea, offshore northern Norway, *in* T. O. Vorren, E. Bergsager, Ø. A. Dahl-Stamnes, E. Holter, B. Johansen, E. Lie, and T. B. Lund, eds., Arctic geology and petroleum potential: Norwegian Petroleum Society Special Publication 2, p. 419–438.
Cecchi, M., J. Markello, and L. Waite, 1995, Sequence stratigraphy architecture of Carboniferous–Permian sedimentary systems of the Norwegian Barents Sea with comparison to coeval systems of the U.S.A., *in* R. J. Steel, V. L. Felt, E. P. Johannessen, and C. Mathieu, eds., Sequence stratigraphy on the northwest European margin: Norwegian Petroleum Society Special Publication 5, p. 545–569.
Choquette, P. W., and N. P. James, 1987, Diagenesis #12. Diagenesis in limestones: 3. The deep burial environment: Geoscience Canada, v. 14, p. 3–35.
Choquette, P. W., and L. C. Pray, 1970, Geological nomenclature and classification of porosity in sedimentary carbonates: AAPG Bulletin, v. 54, p. 207–250.
Choquette, P. W., and R. P. Steinen, 1980, Mississippian nonsupratidal dolomite, Ste. Genevieve Limestone, Illinois basin: Evidence for mixed water dolomitization, *in* D. H. Zenger, J. B. Dunham, and R. L. Ethington, eds., Concepts and models of dolomitization: SEPM Special Publication 28, p. 163–196.
Dawans, J. M., and P. K. Swart, 1988, Textural and geochemical alternations in late Cenozoic Bahamian dolomites: Sedimentology, v. 35, p. 385–403.
Doré, A. G., 1995, Barents Sea geology, petroleum resources and commercial potential: Arctic, v. 48, p. 207–221.
Dunnington, H. V., 1967, Aspects of diagenesis and shape change in stylolitic limestone reservoirs: Proceedings of the Seventh World Petroleum Congress, Mexico City, Mexico: New York, Elsevier, v. 2, p. 339–352.
Ehrenberg, S. N., 1997, Influence of depositional sand quality and diagenesis on porosity and permeability: Examples from Brent Group reservoirs, northern North Sea: Journal of Sedimentary Research, v. 67, p. 197–211.
Ehrenberg, S. N., and T. A. Svånå, 2001, Use of spectral gamma ray signature to interpret stratigraphic surfaces in carbonate strata: An example from the Finnmark carbonate platform (Carboniferous–Permian), Barents Sea: AAPG Bulletin, v. 85, p. 295–308.
Ehrenberg, S. N., H. M. Gjerstad, and F. Hadler-Jacobsen, 1992, Smørbukk field— A gas condensate fault trap in the Haltenbanken Province, offshore mid-Norway, *in* M. T. Halbouty, ed., Giant oil and gas fields of the decade 1978–1988: AAPG Memoir 54, p. 323–348.
Ehrenberg, S. N., E. B. Nielsen, T. A. Svånå, and L. Stemmerik, 1998a, Depositional evolution of the Finnmark carbonate platform, Barents Sea: Results from wells 7128/6-1 and 7128/4-1: Norsk Geologisk Tidsskrift, v. 78, p. 185–224.
Ehrenberg, S. N., E. B. Nielsen, T. A. Svånå, and L. Stemmerik, 1998b, Diagenesis and reservoir quality of the Finnmark carbonate platform, Barents Sea: Results from wells 7128/6-1 and 7128/4-1: Norsk Geologisk Tidsskrift, v. 78, p. 225–251.
Ehrenberg, S. N., N. A. H. Pickard, T. A. Svånå, I. Nilsson, and V. I. Davydov, 2000, Sequence stratigraphy of the inner Finnmark carbonate platform (Upper Carboniferous–Permian), Barents Sea— Correlation between well 7128/6-1 and the shallow IKU cores: Norsk Geologisk Tidsskrift, v. 80, p. 129–161.
Ehrenberg, S. N., N. A. H. Pickard, L. B. Henriksen, T. A. Svånå, P. Gutteridge, and D. Macdonald, 2001, Depositional and sequence stratigraphic model for cold-water, spiculitic strata based on the Kapp Starostin Formation (Permian) of Spitsbergen and equivalent deposits from the Barents Sea: AAPG Bulletin, v. 87, p. 2061–2087.
Ehrenberg, S. N., N. A. H. Pickard, T. A. Svånå, and N. H. Oxtoby, 2002, Cement geochemistry of photozoan carbonate strata (Upper Carboniferous–Lower Permian), Finnmark carbonate platform, Barents Sea: Journal of Sedimentary Research, v. 72, p. 95–115.
Ehrenberg, S. N., G. P. Eberli, M. Keramati, and A. Moallemi, 2004, Porosity differentiation within interbedded limestone-dolostone reservoirs (abs.): 66th European Association of Geoscientists and Engineers Conference and Exhibition, Paris, Paper E004.
Eliassen, A., and M. R. Talbot, 2001, Late Carboniferous gypsum karst in Central Spitsbergen, Svalbard (abs.), *in* U. G. Wortmann and H. Funk, eds.: International Association of Sedimentologists 2001, 21st meeting, Davos, Abstracts and Program, p. 133–134.
Emery, D., J. D. Hudson, J. D. Marshall, and A. D. Dickson, 1988, The origin of late spar cements in the Lincolnshire Limestone, Jurassic of central England: Journal of the Geological Society (London), v. 145, p. 621–633.
Fitchen, W. M., 1997, Carbonate sequence stratigraphy and its application to hydrocarbon exploration and reservoir development, *in* I. Palaz and K. J. Marfurt, eds., Carbonate seismology: Society of Exploration Geophysicists Geophysical Developments Series 6, p. 121–178.
Folk, R. L., and A. Siedlecka, 1974, The ''Schizohaline'' environments: Its sedimentary and diagenetic fabrics as exemplified by late Paleozoic rocks of Bear Island, Svalbard: Sedimentary Geology, v. 11, p. 1–15.
Ford, D., and J. Golonka, 2003, Phanerozoic paleogeography, paleoenvironment and lithofacies maps of the circum-Atlantic margins: Marine and Petroleum Geology, v. 20, p. 249–285.
Grover G., Jr., and J. F. Read, 1983, Paleoaquifer and deep burial cements defined by regional cathodoluminescence patterns, Middle Ordovician carbonates, Virginia: AAPG Bulletin, v. 67, p. 1275–1303.
Harms, J. C., and P. W. Choquette, 1965, Geologic evaluation of a gamma-ray porosity device: Society of Professional Well Log Analysts, Sixth Annual Logging Symposium Transactions, v. 2, paper C, p. 37.
Heald, M. T., 1959, Significance of stylolites in permeable sandstones: Journal of Sedimentary Petrology, v. 29, p. 251–253.
James, N. P., 1997, The cool-water carbonate depositional realm, *in* N. P. James and J. A. D. Clarke, eds., Cool-water carbonates: SEPM Special Publication 56, p. 1–20.
Koepnick, R. B., 1985, Distribution and permeability of stylolite-bearing horizons within a Lower Cretaceous carbonate reservoir in the Middle East: Society of Petroleum Engineers Paper 14173, p. 1–7.
Larssen, G. B., G. Elvebakk, L. B. Henriksen, E. Kristensen, I. Nilsson, T. J. Samuelsberg, T. A. Svånå, L. Stemmerik, and D. Worsley, 2002, Upper Paleozoic lithostratigraphy of the southern Norwegian Barents Sea: http://www.npd.no/Norsk/Produkter+og+tjenester/Publikasjoner/Oversikt+sokkelpublikasjoner/npd+bulletin.htm, (accessed October 1, 2004), 76 p.
Lønøy, A., 1988, Environmental setting and diagenesis of Lower Permian *Palaeoaplysina* buildups and associated sediments from Bjørnøya: Implications for exploration of the Barents Sea: Journal of Petroleum Geology, v. 11, p. 141–156.
Lucia, F. J., 1999, Carbonate reservoir characterization: Springer, Berlin, 226 p.
Martirosyan, V., L. Popova, and M. Vepreva, 1998, The petroleum systems of the Pechora platform foreland, Russia: Petroleum Geoscience, v. 4, p. 339–348.

Mazzullo, S. J., and P. M. Harris, 1992, Mesogenetic dissolution: Its role in porosity development in carbonate reservoirs: AAPG Bulletin, v. 76, p. 607–620.

Meyers, W. J., 1978, Carbonate cements: Their regional distribution and interpretation in Mississippian limestones of southwestern New Mexico: Sedimentology, v. 25, p. 371–400.

Montañez, I. P., J. M. Gregg, and K. L. Shelton, 1997, Basin-wide diagenetic patterns: Integrated petrologic, geochemical, and hydrologic considerations: SEPM Special Publication 57, 302 p.

Moore, C. H., 2001, Carbonate reservoirs porosity evolution and diagenesis in a sequence stratigraphic framework: Amsterdam, Elsevier, 444 p.

Morin, J., A. Desrochers, and B. Beauchamp, 1994, Facies analysis of Lower Permian platform carbonates, Sverdrup Basin, Canadian Arctic Archipelago: Facies, v. 31, p. 105–130.

Muin, A., and Hastowidodo, 1982, Diagenesis and porosity occlusion of stylolitic limestones: An example from the ''x'' well, Arun Limestone: Proceedings of the Joint ASCOPE/CCOP (Association of Southeast Asian Nations Council on Petroleum/Coordinating Committee for Geoscience Programs in East and Southeast Asia) Workshop on the Hydrocarbon Occurrence in Carbonate Rocks: ASCOPE Technical Paper TP/2, p. 235–247.

Murray, R. C., 1960, Origin of porosity in carbonate rocks: Journal of Sedimentary Petrology, v. 30, p. 59–84.

Nilsen, K. T., E. Henriksen, and G. B. Larssen, 1993, Exploration of the late Palaeozoic carbonates in the southern Barents Sea— A seismic stratigraphic study, *in* T. O. Vorren, E. Bergsager, Ø. A. Dahl-Stamnes, E. Holter, B. Johansen, E. Lie, and T. B. Lund, eds., Arctic geology and petroleum potential: Norwegian Petroleum Society Special Publication 2, p. 393–403.

Nyland, B., L. N. Jensen, J. Skagen, O. Skarpnes, and T. Vorren, 1992, Tertiary uplift and erosion in the Barents Sea: Magnitude, timing and consequences, *in* R. M. Larsen, H. Brekke, B. T. Larsen, and E. Talleraas, eds., Structural and tectonic modelling and its application to petroleum geology: Norwegian Petroleum Society Special Publication 1, p. 153–162.

Oelkers, E. H., P. A. Bjørkum, and W. M. Murphy, 1996, A petrographic and computational investigation of quartz cementation and porosity reduction in North Sea sandstones: American Journal of Science, v. 296, p. 1–28.

Olaussen, S., L. Beck, L. M. Fält, E. Graue, K. G. Jacobson, O. A. Malm, and D. South, 1992, Gullfaks field— Norway East Shetland Basin, northern North Sea, *in* N. H. Foster and E. A. Beaumont, compilers, Structural traps VI, Tectonic and nontectonic fold traps: AAPG Treatise of Petroleum Geology, Atlas of Oil and Gas Fields, p. 55–83.

Oldershaw, A. E., and T. P. Scoffin, 1967, The source of ferroan and non-ferroan calcite cements in the Halkin and Wenlock limestones: Geological Journal, v. 5, p. 309–320.

Purser, B. H., 1984, Stratiform stylolites and the distribution of porosity: Examples from the Middle Jurassic limestones of the Paris Basin, *in* Stylolites and associated phenomena: Relevance to hydrocarbon reservoirs: Abu Dhabi National Reservoir Research Foundation Special Publication, p. 203–217.

Purser, B. H., A. Brown, and D. M. Aissaoui, 1994, Nature, origins and porosity in dolomites, *in* B. Purser, M. Tucker, and D. Zenger, eds., Dolomites a volume in honour of Dolomieu: International Association of Sedimentologists Special Publication 21, p. 283–308.

Railsback, L. B., 1993, Lithologic controls on morphology of pressure-dissolution surfaces (stylolites and dissolution seams) in Paleozoic carbonate rocks from the mideastern United States: Journal of Sedimentary Petrology, v. 63, p. 513–522.

Schlager, W., 2004, Fractal nature of stratigraphic sequences: Geology, v. 32, p. 185–188.

Schmoker, J. W., and R. B. Halley, 1982, Carbonate porosity versus depth: A predictable relation for south Florida: AAPG Bulletin, v. 66, p. 2561–2570.

Schofield, K., 1984, Are pressure solution, neomorphism and dolomitization genetically related? *in* Stylolites and associated phenomena: Relevance to hydrocarbon reservoirs: Abu Dhabi National Reservoir Research Foundation Special Publication, p. 183–202.

Steel, R. J., and D. Worsley, 1984, Svalbard's post-Caledonian strata: An atlas of sedimentational patterns and palaeogeographic evolution, *in* A. M. Spencer, E. Holter, S. O. Johnsen, A. Mørk, E. Nysæther, P. Songstand, and Å. Spinnangr, eds., Petroleum geology of the north European margin: Norwegian Petroleum Society, London, Graham & Trotman, p. 109–135.

Stemmerik, L., G., 2000, Late Paleozoic evolution of the North Atlantic margin of Pangea: Palaeogeography, Palaeoclimatology, Palaeoecology, v. 161, p. 95–126.

Stemmerik, L., and G. B. Larssen, 1993, Diagenesis and porosity evolution of Lower Permian *Palaeoaplysina* build-ups, Bjørnøya: An example of diagenetic response to high frequency sea level fluctuations in an arid climate, *in* A. D. Horbury and A. D. Robinson, eds., Diagenesis and basin development: AAPG Studies in Geology 36, p. 199–211.

Stemmerik, L., G. Elvebakk, and D. Worsley, 1999, Upper Palaeozoic carbonate reservoirs on the Norwegian Arctic shelf: Delineation of reservoir models with application to the Loppa high: Petroleum Geoscience, v. 5, p. 173–187.

Tucker, M. E., and V. P. Wright, 1990, Carbonate sedimentology: London, Blackwell Scientific Publications, 482 p.

Weyl, P. K., 1959, Pressure solution and the force of crystallization— A phenomenological theory: Journal of Geophysical Research, v. 64, p. 2001–2025.

Wong, P. K., and A. Oldershaw, 1981, Burial cementation in the Devonian Kaybob reef complex, Alberta, Canada: Journal of Sedimentary Petrology, v. 51, p. 507–520.